

**ZONGULDAK BÜLENT ECEVİT UNIVERSITY
GRADUATE SCHOOL OF NATURAL AND APPLIED SCIENCES**

**TIME SERIES ANALYSIS OF SENTINEL 2A/B MULTISPECTRAL IMAGERY
OVER SELECTED LAND COVER LAND USE (LULC) TYPES**



DEPARTMENT OF GEOMATICS ENGINEERING

MASTER OF SCIENCE THESIS

OYA BURCU AKGÜL

APRIL 2019

**ZONGULDAK BÜLENT ECEVİT UNIVERSITY
GRADUATE SCHOOL OF NATURAL AND APPLIED SCIENCES**

**TIME SERIES ANALYSIS OF SENTINEL 2A/B MULTISPECTRAL IMAGERY
OVER SELECTED LAND COVER LAND USE (LULC) TYPES**

DEPARTMENT OF GEOMATICS ENGINEERING

MASTER OF SCIENCE THESIS

Oya Burcu AKGÜL

ADVISOR: Prof. KAZIMIERZ BECEK

ZONGULDAK

April 2019

APPROVAL OF THE THESIS:

The thesis entitled “Time Series Analysis of Sentinel 2A/B Multispectral Imagery over Selected Land Cover Land Use (LULC) Types” and submitted by Oya Burcu AKGÜL has been examined and accepted by the jury as a Master of Science thesis in Department of Geomatics Engineering, Graduate School of Natural and Applied Sciences, Zonguldak Bülent Ecevit University 22/04/2019.

Advisor: Prof. Kazimierz BECEK

Zonguldak Bülent Ecevit University, Faculty of Engineering, Department of Geomatics

Member: Assoc. Prof. Saygın ABDİKAN

Zonguldak Bülent Ecevit University, Faculty of Engineering, Department of Geomatics

Member: Assoc. Prof. Füsün BALIK ŞANLI

Yildiz Technical University, Faculty of Civil Engineering, Department of Geomatic Engineering

Approved by the Graduate School of Natural and Applied Sciences.

.../.../2019

Prof. Ahmet ÖZARSLAN

Director

“With this thesis it is declared that all the information in this thesis is obtained and presented according to academic rules and ethical principles. Also as required by academic rules and ethical principles all works that are not result of this study are cited properly.”


Oya Burcu AKGÜL

ABSTRACT

Master of Science Thesis

TIME SERIES ANALYSIS OF SENTINEL 2A/B MULTISPECTRAL IMAGERY OVER SELECTED LAND COVER LAND USE (LULC) TYPES

Oya Burcu AKGÜL

**Zonguldak Bülent Ecevit University
Graduate School of Natural and Applied Sciences
Department of Geomatics Engineering**

Thesis Advisor: Prof. Kazimierz BECEK

April 2019, 65 pages

Land use and land cover (LULC) varies over time depending on anthropogenic, natural and predominantly seasonal factors. These LULC changes, especially those of permanent type, impact many various natural processes, including agricultural production, and climate change. Therefore, it is very important to systematically and accurately monitor these changes and associated consequences for the natural environment and human existence. Remote sensing provide means to perform these tasks in an effective fashion. This study aims at identifying temporal variations of the Normalised Difference Vegetation Index (NDVI) of selected LULC types.

The selected LULC types are represented by test regions and lines manually extracted from natural colour satellite images. Some of these LULC classes are not changing over time, e.g. roofs of large structures. Hence, time series of spectral index for these classes should not vary significantly. Potentially observed variations are probably caused by inaccuracies in the

ABSTRACT (continued)

calibration of the satellite data and variations in meteorological conditions (translucency of the atmosphere). The level of variations of the NDVI or any other spectral index of “stable” LULC classes could provide information about the accuracy of classification of other LULC classes.

As an Area of Interest (AOI) Bursa-Gemlik region, Turkey has been chosen and analyzed with Sentinel 2 satellite imagery. An approximately monthly sequence of 13 images captured in during 2017 have been used in this study. The changes in NDVI values for each class were interpreted, with auxiliary information such as climate, meteorological data, agricultural production in the region. Six different LULC classes have been investigated including roads, buildings, industrial area, agricultural area, forest and water body. It was found that indeed there are significant differences in the magnitude of variations of the NDVI for investigated sample of selected LULC types.

Keywords: Time series analysis, Land use, Land cover, LULC, Sentinel 2, NDVI, Calibration

Science Code: 616.02.00

ÖZET

Yüksek Lisans Tezi

ARAZİ ÖRTÜSÜ VE ARAZİ KULLANIMI (LULC) TÜRLERİ ÜZERİNE SENTİNEL 2A/B ÇOK SPEKTRUMLU GÖRÜNTÜLERİN ZAMAN SERİLERİ ANALİZİ

Oya Burcu AKGÜL

Zonguldak Bülent Ecevit Üniversitesi

Fen Bilimleri Enstitüsü

Geomatik Mühendisliği Anabilim Dalı

Tez Danışmanı: Prof. Dr. Kazimierz BECEK

Nisan 2019, 65 sayfa

Arazi kullanımı ve arazi örtüsü (LULC), antropojenik, doğal ve ağırlıklı olarak mevsimsel faktörlere bağlı olarak zamanla değişmektedir. Bu arazi örtüsü ve kullanımı değişimleri, özellikle kalıcı tipte olanlar, tarımsal üretim ve iklim değişikliği dahil olmak üzere birçok doğal süreci etkiler. Bu nedenle, doğal çevre ve insan yaşamı için bu değişiklikleri ve ilgili sonuçları sistematik ve doğru bir şekilde izlemek çok önemlidir. Uzaktan algılama, bu görevleri etkili bir şekilde gerçekleştirmek için araçlar sağlar. Bu çalışma seçilen LULC tiplerinin Normalize Edilmiş Fark Bitki Örtüsü İndeksi (NDVI) değerlerinin zamansal değişimlerini tanımlamayı amaçlamaktadır.

Seçilen LULC tipleri, doğal renkli uydu görüntülerinden manuel olarak seçilen hat ve test alanları ile temsil edilmiştir. Bu LULC sınıflarından bazıları zaman içinde değişmemektedir, örneğin; büyük yapıların çatıları gibi. Dolayısıyla, bu sınıflar için spektral indeksin zaman serileri önemli ölçüde değişmemektedir. Potansiyel olarak gözlenen değişikliklere muhtemelen

ÖZET (devam ediyor)

uydu verilerinin kalibrasyonundaki hatalar ve meteorolojik koşullardaki değişiklikler (atmosferin yarı saydamlığı) neden olabilir. “Kararlı” LULC sınıflarının NDVI ya da herhangi bir spektral indeksindeki değişim seviyesi, diğer LULC sınıflarının sınıflandırılma doğruluğu hakkında bilgi sağlayabilir.

İlgi Alanı (AOI) olarak Bursa-Gemlik bölgesi seçilmiş ve Sentinel 2 uydu görüntüleri ile analiz edilmiştir. Bu çalışmada, yaklaşık olarak aylık olarak, 2017 yılında çekilen 13 resim dizisi kullanılmıştır. Her sınıf için NDVI değerindeki değişiklikler, iklim, meteorolojik veriler ve bölgedeki tarımsal üretim gibi yardımcı bilgilerle yorumlanmıştır. Yollar, binalar, sanayi bölgesi, tarım alanı, orman ve su kütlesi olmak üzere altı farklı LULC sınıfı incelenmiştir. Seçilen LULC tiplerinin araştırılmış örnekleri için NDVI değişimlerinin büyüklüğünde önemli farklılıklar olduğu tespit edilmiştir.

Anahtar Kelimeler: Zaman serileri analizi, Arazi kullanımı, Arazi örtüsü, LULC, Sentinel 2, NDVI, Kalibrasyon

Bilim Kodu: 616.02.00

ACKNOWLEDGEMENTS

Above all, I would like to express my gratitude to have experienced the privilege of working with Prof. Kazimierz BECEK. He has guided my thesis with different perspectives and knowledge and made important contributions. I am also grateful from him to give me a vision and change my point of view.

I would like to express my gratitude to Assoc. Prof. Saygın ABDİKAN and Assoc. Prof. Füsün BALIK ŞANLI who contributed to my thesis defense with their valuable comments and suggestions.

I would like to thank Dr. Çağlar BAYIK for his assistance in the implementation of the study.

I would like to thank my husband Volkan AKGÜL, who has spent so many effort for me with his patience, kindness and support during this process.

Finally, I want to expresses my gratefulness to my family who supported my decisions in every conditions. I believe that I have an honourable life with the contributions of them.



TABLE OF CONTENTS

	<u>Page</u>
APPROVAL OF THE THESIS:	ii
ABSTRACT	iii
ÖZET	v
ACKNOWLEDGEMENTS	viii
TABLE OF CONTENTS	ix
LIST OF FIGURES	xi
LIST OF TABLES	xiii
LIST OF SYMBOLS AND ABBREVIATIONS	xv
CHAPTER 1 INTRODUCTION	1
1.1 BACKGROUND	1
1.2 AIM, OBJECTIVES AND SCOPE	2
1.2.1 Aim	2
1.2.2 Objective	2
1.2.3 Scope	3
1.3 LITERATURE REVIEW	3
1.4 SENTINEL 2	5
1.4.1 Overview	5
1.4.2 Mission Objectives	6
1.4.3 Ground Segment	6
1.4.4 Applications	8
1.4.5 Product Types	9
1.5 CONTENTS	10

TABLE OF CONTENTS (continued)

	<u>Page</u>
CHAPTER 2 BASIC PRINCIPLES OF REMOTE SENSING	11
2.1 ELECTROMAGNETIC SPECTRUM	13
2.2 SPECTRAL RADIANCE PROPERTIES OF OBJECTS	14
2.2.1 Spectral Reflection of Plants	14
2.2.2 Spectral Reflection of Ground Surface	15
2.2.3 Spectral Reflection of Water	15
2.2.4 Spectral Radiation of Surface Bodies	15
CHAPTER 3 DIGITAL IMAGE PROCESSING TECHNIQUES	17
3.1 DIGITAL IMAGE	17
3.2 RESOLUTION OF A REMOTE SENSING IMAGE	18
3.2.1 Spectral Resolution	18
3.2.2 Spatial Resolution	19
3.2.3 Radiometric Resolution	20
3.2.4 Temporal Resolution	21
3.3 IMAGE CLASSIFICATION	21
3.3.1 Pixel-Based Classification	22
3.3.1.1 Supervised Classification	22
3.3.1.1.1 Maximum likelihood method	23
3.3.1.1.2 Paralel lepiped method	23
3.3.1.1.3 Minimum distance method	24
3.2.1.2 Unsupervised Classification	24
3.3.2 Object-Based Classification	25
CHAPTER 4 DATA AND METHODS	29
4.1 STUDY AREA	29
4.2 DATA	35
4.2.1 NDVI	35

TABLE OF CONTENTS (continued)

	<u>Page</u>
4.2.2 Data Analysis Steps	36
CHAPTER 5 RESULTS AND DISCUSSION	43
5.1 RESULTS	43
5.1.1 NDVI Results of the Road Type Land Cover Class	43
5.1.2 NDVI Results of the Industrial Area Type Land Cover Class	45
5.1.3 NDVI Results of the Forest Type Land Cover Class	47
5.1.4 NDVI Results of the Buildings Type Land Cover Class	49
5.1.5 NDVI Results of the Agricultural Area Type Land Cover Class	51
5.1.6 NDVI Results of the Sea Type Land Cover Class	53
5.2 DISCUSSION	55
CHAPTER 6 CONCLUSION	59
REFERENCES	61
CURRICULUM VITAE	65



LIST OF FIGURES

<u>No</u>	<u>Page</u>
Figure 1.1 Copernicus Ground Segment Architecture	7
Figure 2.1 A 3D model of electromagnetic wave.	11
Figure 2.2 Electromagnetic energy and spectral interaction	12
Figure 2.3 The Electromagnetic Spectrum.....	13
Figure 3.1 Elements of Digital Image.	17
Figure 3.2 Natural Color Combinations.....	19
Figure 3.3 The spatial resolutions of the Landsat (30 m) vs. the IKONOS image (4 m).	20
Figure 3.4 Radiometric resolution sample.	21
Figure 3.5 Illustration of the maximum likelihood method.	23
Figure 3.6 Illustration of the paralel lepiped method.	24
Figure 3.7 Minimum distance classifier.....	24
Figure 4.1 Topography of AOI, Gemlik.	30
Figure 4.2 Daily parameter of rain at 2017 in Gemlik.....	30
Figure 4.3 Daily parameter of temperature at 2017 in Gemlik.	31
Figure 4.4 Calculation of NDVI imagery with ArcGIS.....	36
Figure 4.5 Composite image.	36
Figure 4.6 True Color composite bands creation.	37
Figure 4.7 Defining the land cover types in ArcGIS.....	38
Figure 4.8 Polygon selection of shapefiles.....	38
Figure 4.9 Polyline selection of shapefiles.....	39
Figure 4.10 Raster to point conversion.	39
Figure 4.11 Creating polygon features union.....	40
Figure 4.12 Creating polyline features dissolve.....	40
Figure 4.13 Point data join to the shapefiles.	41
Figure 4.14 Open attribute table.....	41
Figure 4.15 Attribute table data sample for Sea, Feb 2017.....	42
Figure 5.1 Time series of NDVI for the Road type class.	44

LIST OF FIGURES (continued)

<u>No</u>	<u>Page</u>
Figure 5.2 Standard deviation (SD) time series analysis of NDVI for the Road type class. ...	45
Figure 5.3 Time series analysis of NDVI for the Industrial Area type land cover class.....	46
Figure 5.4 SD time series analysis of NDVI for the Industrial Area type class.....	47
Figure 5.5 Time series analysis of NDVI for the Forest type land cover class.....	48
Figure 5.6 SD time series analysis of NDVI for the Forest type class.....	49
Figure 5.7 Time series analysis of NDVI for the Buildings type land cover class.	50
Figure 5.8 SD time series analysis of NDVI for the Buildings type class	50
Figure 5.9 Time series analysis of NDVI for the Agricultural Area type land cover class.	52
Figure 5.10 SD time series analysis of NDVI for the Agricultural Area type class.	52
Figure 5.11 Time series analysis of NDVI for the Sea type land cover class.....	54
Figure 5.12 SD time series analysis of NDVI for the Sea type class.....	54
Figure 5.13 Time series of average NVDI of classes.....	56

LIST OF TABLES

<u>No</u>	<u>Page</u>
Table 1.1 Spectral bands for the Sentinel-2 sensors.....	9
Table 1.2 Sentinel 2 product types.	10
Table 4.1 Distribution of agricultural land usage in Gemlik.....	32
Table 4.2 Product types of Fruit and Spice Plants in Gemlik.	33
Table 4.3 Product types of Vegetables in Gemlik.....	33
Table 4.4 Product types in Cereals And Other Herbal Products in Gemlik, 2017.....	34
Table 4.5 Monthly attribute table of Sea.	42
Table 5.1 Attribute table of Road type class	44
Table 5.2 Attribute table of Industrial Area type land cover class.....	46
Table 5.3 Attribute table of Forest type land cover class.....	48
Table 5.4 Attribute table of Buildings type land cover class.	49
Table 5.5 Most common products of Agricultural Area in Gemlik.....	51
Table 5.6 Attribute table of Agricultural Area type land cover class	51
Table 5.7 Attribute table of Sea type land cover class.	53



LIST OF SYMBOLS AND ABBREVIATIONS

SYMBOLS

c	: Light Velocity
E	: Electric wave
B	: Magnetic wave
v	: Distance
λ	: Wavelength
f	: Wave frequency
μm	: Micrometer
km	: Kilometer
mm	: Milimeter
$^{\circ}\text{C}$: Centigrade degree
%	: Percentage
N	: North
E	: East
a	: Intensity
x	: Actual Coordinates of the Image
y	: Actual Coordinates of the Image
m	: Meter

ABBREVIATIONS

3D	: 3 Dimensional
AIC	: Akaike Information Criteria
AOI	: Area of Interest
Avg	: Average
Avg. Max.	: Average Maximum
Avg. Min.	: Average Minimum

LIST OF SYMBOLS AND ABBREVIATIONS (continued)

Avg. SD	: Average Standard Deviation
B2	: Blue Band
B3	: Green Band
B4	: Red Band
B8	: Near Infrared Band
FBE	: Fen Bilimleri Enstitüsü
GIS	: Geographical Information Systems
IFOV	: Instantaneous Field of View
LULC	: Land Use Land Cover
Max	: Maximum
Min	: Minimum
NDVI	: Normalized Difference Vegetation Index
NIR	: Near Infrared
RGB	: Red, Green, Blue
SD	: Standard Deviation
USD	: United States Dollars
ZBEÜ	: Zonguldak Bülent Ecevit Üniversitesi

CHAPTER 1

INTRODUCTION

1.1 BACKGROUND

Remote Sensing is the art and science of extracting information about the environment from electromagnetic waves which are reflected from the earth by the sensing systems. The term “remote sensing” describes remote position of the observer from the sensor, and not the remote position of the sensor from the surface of the earth.

The World War I (1914-1918) was the period when aerial photography was significantly advanced. This period witnessed also important studies in the invisible ranges of the electromagnetic spectrum. The Second World War (1939-1945) period when the development of the aerial photography gained the highest momentum. In 1960 the first world observation satellite TRIOS was sent to space. During that time, the airborne observation technologies based on the infrared and microwave ranges progressed significantly. The term Remote Sensing was coined by Dr. Evelyn Pruitt in late 1950s.

The first remote sensing program started with the launch of LANDSAT in 1972, which has been still continuing. The Landsat satellite is the first multi-band satellite enabling the systematic and continuous observation of the earth's surface. The Landsat program significantly stimulated development of digital data processing techniques and image processing tools.

Remote sensing has been developed primarily for military purposes. However, soon after more research has been centered on civilian applications of this technology. In particular, observation of vegetation, water and air pollution can be given as an example. Remote Sensing data sets can be used to observe both spatial and temporal change.

Important applications of remote sensing technology can be listed as follows (Schowengerdt 1997);

1. Environmental assessment and monitoring (irregular urbanization, hazardous wastes)
2. Identification and visualization of global change (atmospheric ozone depletion, deforestation, global warming)
3. Agriculture (product status, harvest estimation, soil erosion)
4. Investigation of non-renewable resources (minerals, oil, natural gas)
5. Renewable natural resources (wetlands, land, forests, oceans)
6. Meteorology (atmospheric dynamics, weather forecasting)
7. Cartography (topography, land use, engineering)
8. Military surveillance and discovery (strategic policies, tactical assessment)
9. Mass media (examples, analysis).

1.2 AIM, OBJECTIVES AND SCOPE

1.2.1 Aim

The goal of this study is to improve the knowledge and skills of the usage of temporal and multispectral remote sensing type of data for land use and land cover (LULC) analysis. The Copernicus Sentinel-2A/B data are used in this study. These data with their high temporal and spatial resolution constitute a major asset for many type of environmental and societal applications.

1.2.2 Objective

The main objectives of this study leading to the above specified goal are:

- (i) selecting samples representing different LULC classes using photo interpretation of a true color image and evaluating;
- (ii) performing the time series analysis of the selected sample areas by taking advantage of the temporal resolution of Sentinel 2A/B satellite images;
- (iii) relating the temporal changes of defined areas with meteorological data, vegetation cover, structural characteristics of objects and other parameters.

1.2.3 Scope

In this study the following LULC classes are considered:

- Water body (Sea);
- Agriculture (Fruits, Vegetables, Cereals etc.);
- Buildings (from Urban area, Rural area and Coastline);
- Roads (Asphalt, Surface treatment and Unpaved),
- Industrial areas and
- Forests (Evergreen trees and Deciduous trees).

The study focuses on a period from January 2017 to January 2018. The Sentinel 2A/B multispectral data are used in this project, and in particular band 4 (Red) and 8 (NIR).

Using the above mentioned data one of the most popular spectral index is used which is the Normalised Difference Vegetation Index (NDVI). The period of observations (approximately one year) did not allow to detect possible interannual trends in the time series, due to climate change.

1.3 LITERATURE REVIEW

Remote sensing is the science of acquiring information about the earth surface through data received by sensor systems. Remote sensing technologies are based on the principle of receiving, recording, processing and using information emitted or reflected by the earth's surface in a form of electromagnetic waves. In the 1960s, remote sensing technology was first initiated in order to gather intelligence data. It was started to be used for civilian purposes through the Landsat program of satellites developed by the United States in early 1970s (Çölkesen 2009). The Remote sensing technology has been used in many branches of sciences, including hydrology, agriculture, geology, mining, forestry, natural resources, land cover monitoring, detection of illegal structures, detection of damages of natural structures, foundation for land management plans and urban planning activities. The benefits of remote sensing include an instant view of large areas, low cost, fast data transfer and accurate information in a short time.

Selected relevant publications for this study include: Acker et. al. (2009) obtained time series showing the chlorophyll content in seaside affected by rivers from SeaWiFS images.

Çelik (2006) conducted spatial data analysis with the remote sensing data of Istanbul Sarıyer District. In this study, image processing techniques are used on satellite images and vector data of 1998, 2001 and 2005. As a result of the study, it has been observed that there is a decrease in the woodland and empty areas in parallel with the increase of settlement areas and roads.

Immitzer et. al. (2016) aimed to map crop species and tree species with Sentinel 2. It presents the preliminary results of two classification exercises that assess the characteristics of their data. The first case study deals with mapping of some crops and bare lands in Austria, while the second case study aims to map different types of deciduous and coniferous tree species in Germany. For tree species and product types, respectively 65% and 76% accuracy were obtained.

In their study, Inglada et. al. (2015) aims to assess the extent to which the most advanced supervised classification methods can be applied to high-resolution multi-temporal optical images to produce accurate crop-type maps on a global scale. The results show that a random forest classifier working on linearly filled images with transient intervals can achieve over 80% overall accuracy for most sites. The approach is based on supervised machine learning techniques that need to collect on-site data for the training phase, but the map production is completely automated.

Song et. al. (2017) evaluated the detection of cotton root rot with 10 m resolution Sentinel-2A satellite images and compared the results with multi spectral airborne images using unsupervised classification at both the field and regional levels. The accuracy evaluation showed that the classification maps from the Sentinel-2A images had an accuracy of 94.1% for the site subset images and 91.2% for the whole image compared to the airborne image classification results.

Rapinel et. al. (2019) discusses the advantages of the Sentinel-2 time series to distinguish plant communities in wet meadows. The annual Sentinel-2 time series was compared with single date and single-band data sets derived from this time series for mapping of grassland plant communities in a temperate floodplain near Mont-Saint-Michel Bay. Satellite images were

classified using support vector machine (SVM) and random forest (RF) classifiers. The results show that the SVM classifier performs slightly better than the RF classifier (0.78 and 0.71, respectively).

Belgiu and Csillik (2018) mapped the crop from Sentinel-2 time series data using objects as spatial analysis units. The Sentinel-2 time series data stack was automatically partitioned using the multi-resolution segmentation algorithm and the resulting image objects were classified using the Time-Weighted Dynamic Time-Solving (TWDTW) method. The applied cultivation area mapping frame gave an overall accuracy of 93.43% and a kappa index of 92%. It has the advantage of creating a spatial vector data set that supports decision-making in various agricultural management contexts.

1.4 SENTINEL 2

The Copernicus Sentinel-2 mission comprises a constellation of two polar-orbiting satellites placed in the same sun-synchronous orbit, phased at 180° to each other. It aims at monitoring variability in land surface conditions, and its wide swath width (290 km) and high revisit time (10 days at the equator with one satellite, and 5 days with 2 satellites under cloud-free conditions which results in 2-3 days at mid-latitudes) will support monitoring of Earth's surface changes. The coverage limits are from between latitudes 56° south and 84° north (URL-1 2019).

1.4.1 Overview

As part of the European Copernicus program, Sentinel-2A was successfully released on 23 June 2015, and the first images were taken a few days later (URL-2 2019). Sentinel-2 (S2) carries an innovative wide-swath, high-resolution, multispectral imager (MSI) with 13 spectral bands. This will offer unexampled perspectives to our lands and vegetation (from Drusch et. al. 2012, URL-3 2018). The full tasks of the twin satellites moving in the same orbit but phased at 180°, is designed to give 5-days high revisit rate at the Ecuador. SENTINEL-2 contains 13 bands in different spatial resolution which are four bands at 10 m, six bands at 20 m and three bands at 60 m. SENTINEL-2 is a wide-swath, high-resolution, multi-spectral imaging mission. Copernicus allows monitoring of vegetation, soil and water cover, as well as monitoring of inland waterways and coastal areas.

The data obtained, the scope of the task and the high frequency of repetition provide geographic information at local, regional, national and international scales. The data obtained is designed to be modified and adapted by users interested in the following thematic areas:

- spatial planning
- agro-environmental monitoring
- water cover monitoring
- forest and vegetation monitoring
- land carbon, natural resource monitoring
- global crop monitoring

1.4.2 Mission Objectives

SENTINEL-2 mission objectives are to provide:

- systematic global gains of high-resolution, multi-spectral images with high repetition frequency
- continuity of multi-spectral imagery provided by the SPOT series of satellites and the USGS LANDSAT Thematic Mapper instrument
- observation data for the next generation of operational products, such as land-cover maps, land-change detection maps and geophysical variables.

SENTINEL-2 is expected to contribute significantly to Copernicus themes such as climate change, land monitoring, emergency management and security.

With its 13 spectral bands, 290 km swath width and high revisit frequency, SENTINEL-2's MSI instrument supports a wide range of land studies and programmes, and reduces the time required to build a European cloud-free image archive. The spectral bands of SENTINEL-2 will provide data for land cover/change classification, atmospheric correction and cloud/snow separation.

1.4.3 Ground Segment

The ground segment consists of the Core Ground Segment, the Collaborative Ground Segment and the Copernicus contributing missions' ground segments (Figure 1.1).

The main purpose of core ground segment is monitoring and controlling the SENTINEL spacecraft, ensuring the measurement data acquisition, processing, archiving and dissemination to the final users. Additionally, it is responsible for performing conflict-free mission planning according to a pre-defined operational scenario, and ensures the quality of data products and performance of the space-borne sensors by continuous monitoring, calibration and validation activities, guaranteeing the overall performance of the mission.

Calibration is used to assess the response of the instrument, and to ensure that the changes that occur naturally over time in systems and hardware are managed to ensure stability of output. Having undergone calibration, the processed data requires validation. Validation is confirmation of the correct adoption of the calibrations performed, and that the subsequent processing is fit for dissemination to the user community.

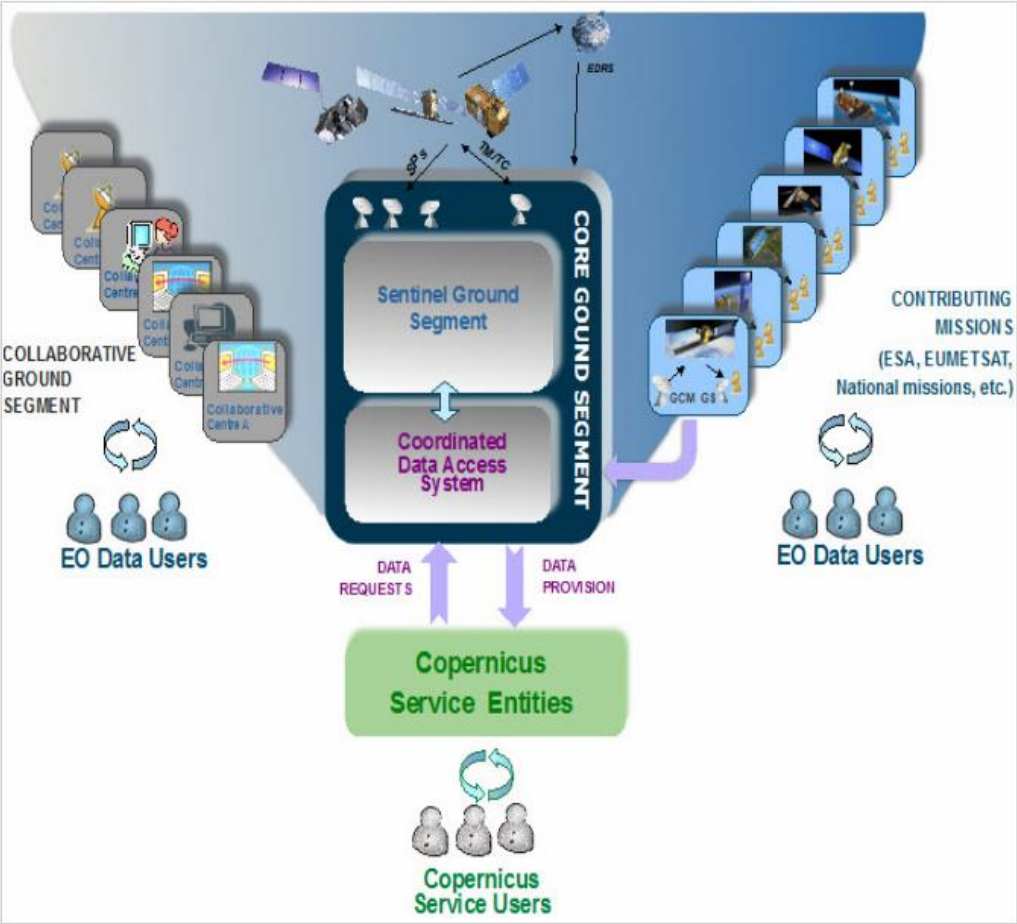


Figure 1.1 Copernicus Ground Segment Architecture (from URL-4 2019).

The Copernicus ground segment is complemented by the Sentinel collaborative ground segment, which was introduced with the aim of exploiting the Sentinel missions further. This

entails additional elements for specialised solutions in different technological areas such as data acquisition, complementary production and dissemination, innovative tools and applications, and complementary support to calibration and validation activities.

The Copernicus contributing mission ground segments, with their own specific control functions, data reception, data processing, data dissemination and data archiving facilities, deliver essential data complementing the Sentinel missions.

1.4.4 Applications

Sentinel-2 serves a wide range of applications related to Earth's land and coastal water. The mission provides information for agricultural and forestry practices and for helping manage food security. Satellite images are used to determine various plant indices such as leaf area chlorophyll and water content indexes. This is particularly important for effective yield prediction and applications related to Earth's vegetation.

As well as monitoring plant growth, Sentinel-2 can be used to map changes in land cover and to monitor the world's forests. It also provides information on pollution in lakes and coastal waters. Images of floods, volcanic eruptions and landslides contribute to disaster mapping and help humanitarian relief efforts.

Examples for applications include:

- Monitoring land cover change for environmental monitoring
- Agricultural applications, such as crop monitoring and management to help food security
- Detailed vegetation and forest monitoring and parameter generation (e.g. leaf area index, chlorophyll concentration, carbon mass estimations)
- Observation of coastal zones (marine environmental monitoring, coastal zone mapping)
- Inland water monitoring
- Glacier monitoring, ice extent mapping, snow cover monitoring
- Flood mapping & management (risk analysis, loss assessment, disaster management during floods)

The Sentinel Monitoring web application offers an easy way to observe and analyse land changes based on archived Sentinel-2 data.

1.4.5 Product Types

The MSI measures the Earth's reflected radiance in 13 spectral bands from VNIR to SWIR (Table 1.1). The Bandwidth (nm) is measured at Full Width Half Maximum (FWHM).

Products are a compilation of elementary granules of fixed size, within a single orbit. A granule is the minimum indivisible partition of a product (containing all possible spectral bands).

For Level-1C and Level-2A, the granules, also called tiles, are 100x100km² ortho-images in UTM/WGS84 projection. The UTM (Universal Transverse Mercator) system divides the Earth's surface into 60 zones. Each UTM zone has a vertical width of 6° of longitude and horizontal width of 8° of latitude. Tiles are approximately 600 MB in size. Tiles can be fully or partially covered by image data. Partially covered tiles correspond to those at the edge of the swath.

Table 1.1 Spectral bands for the Sentinel-2 sensors.

Sentinel-2 bands	Sentinel-2A		Sentinel-2B		Sentinel 2A/B
	Central wavelength (nm)	Bandwidth (nm)	Central wavelength (nm)	Bandwidth (nm)	Spatial resolution (m)
Band 1 – Coastal aerosol	442.7	21	442.2	21	60
Band 2 – Blue	492.4	66	492.1	66	10
Band 3 – Green	559.8	36	559.0	36	10
Band 4 – Red	664.6	31	664.9	31	10
Band 5 – Vegetation red edge	704.1	15	703.8	16	20
Band 6 – Vegetation red edge	740.5	15	739.1	15	20
Band 7 – Vegetation red edge	782.8	20	779.7	20	20
Band 8 – NIR	832.8	106	832.9	106	10
Band 8A – Narrow NIR	864.7	21	864.0	22	20
Band 9 – Water vapour	945.1	20	943.2	21	60
Band 10 – SWIR – Cirrus	1373.5	31	1376.9	30	60
Band 11 – SWIR	1613.7	91	1610.4	94	20
Band 12 – SWIR	2202.4	175	2185.7	185	20

Sentinel-2 products available for users (either generated by the ground segment or by the Sentinel-2 Toolbox) are listed in Table 1.2.

Table 1.2 Sentinel 2 product types.

Name	High-level Description	Production & Distribution	Data Volume
Level-1C	Top-of-atmosphere reflectances in cartographic geometry	Systematic generation and on-line distribution	600 MB (each 100x100 km ²)
Level-2A	Bottom-of-atmosphere reflectance in cartographic geometry	Systematic generation and on-line distribution and generation on user side (using Sentinel-2 Toolbox)	800 MB (each 100x100 km ²)

1.5 CONTENTS

In this thesis, time series analysis of different type of classes using with Sentinel 2 imagery is handled. Chapter 2 will present basic principles of remote sensing. This section introduces information about electromagnetic spectrum. It is followed by the digital image processing techniques in Chapter 3. While data and methods are taking part in Chapter 4, result and discussion part in Chapter 5 investigates the time depended change analysis of different classes. Finally, Chapter 6 includes the conclusion part which gives general interpretation of the results of the study.

CHAPTER 2

BASIC PRINCIPLES OF REMOTE SENSING

The satellite images are photographic or digital representations of the earth. A digital image may also be in the form of a written record in magnetic medium or in the form of digital information in a computer memory.

The quantity used in remote sensing is the electromagnetic energy (EE) emitted or reflected from the object of interest. This energy encompasses all forms of energy that act in the form of sinusoidal and harmonic waves with light velocity(c).

The Sun and various natural or artificial sources emit electromagnetic energy at different wavelengths. The visible light is just a narrow slot of possible electromagnetic radiation ranges that are around us. All E follows the wave theory developed by Maxwell. According to this theory, the electromagnetic wave components are a sinusoidal electric wave (E) and magnetic wave (B), both of which are perpendicular to the direction of propagation as shown in Figure 2.1.

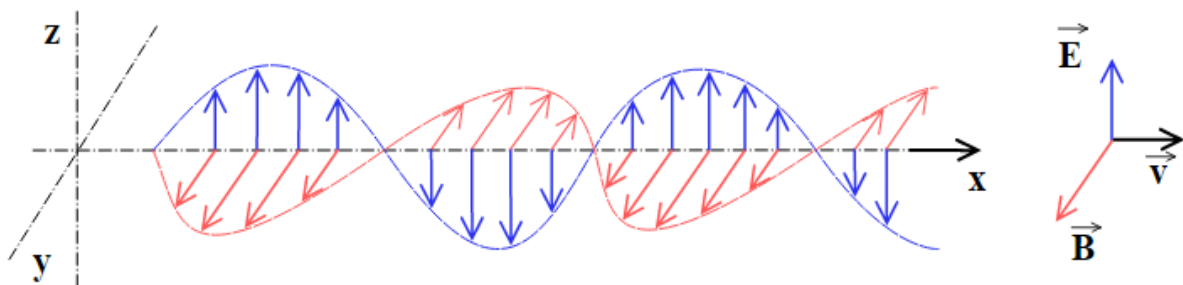


Figure 2.1 A 3D model of electromagnetic wave.

Where the E, B and v represents the electric, magnetic field and propagation velocity and direction, respectively. The distance between subsequent maximum/minimum values of electric or magnetic field is the λ "wavelength", and the number of waves passing through a fixed point

in space per unit time (second) is f "wave frequency". In basic physics, the general equality of the waves is:

$$c = f \cdot \lambda \quad (2.1)$$

where c is the speed of propagation of the electromagnetic wave; f is the frequency (Hz), and λ is the wave length.

The main components of a remote sensing system are the source of electromagnetic energy, interaction with the earth, interaction with the atmosphere, and the sensor (Fig.2.2)

- a) Source: Sunlight, natural radiation or artificial electromagnetic radiation may be the source of electromagnetic radiation.
- b) Interaction with the Earth: The amount of radiation reflected from the Earth depends on the characteristics of the objects on earth.
- c) Interaction with the atmosphere: Electromagnetic energy undergoes scattering and degradation with various effects as it passes through the atmosphere.
- d) Sensor: Electromagnetic radiation is recorded by a sensor.

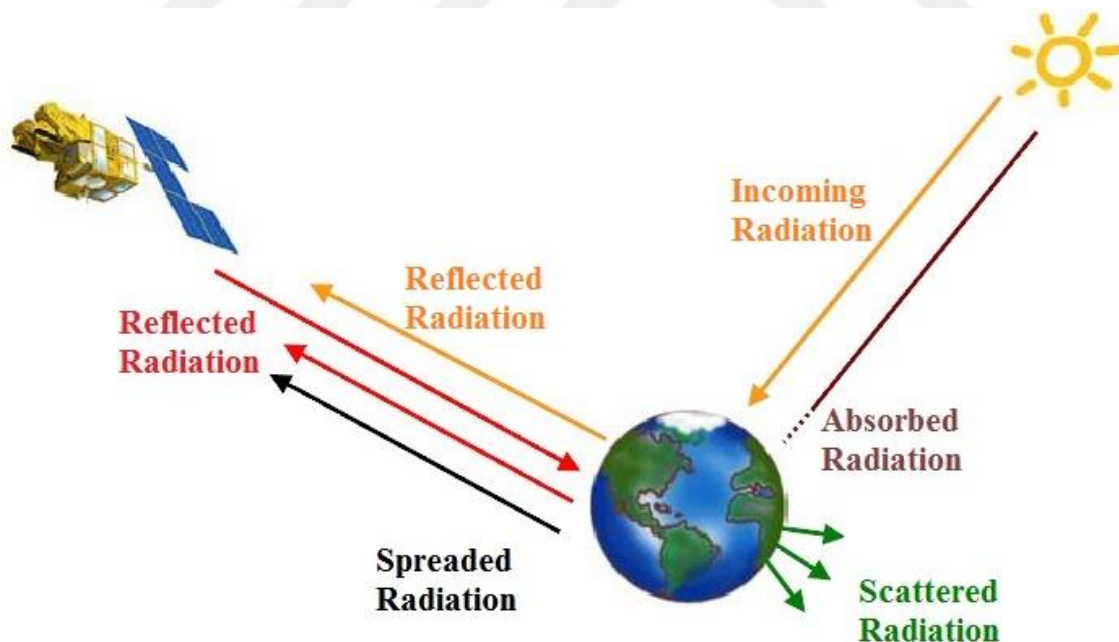


Figure 2.2 Electromagnetic energy and spectral interaction.

2.1 ELECTROMAGNETIC SPECTRUM

Remote sensing is the science and technology of acquiring information about objects, using electromagnetic waves. Nowadays, remote sensing data are collected by aircraft or satellite platforms, which are equipped with sensors. Cameras and sensors form images by measuring the amount of energy reflected and emitted from the earth in the electromagnetic spectrum. Electromagnetic waves are frequently considered as wave bands or spectrum. A band is also frequently referred to as channel, is named for a specific part of the electromagnetic spectrum. Figure 2.3 shows spectrum of electromagnetic waves. A narrow part of the spectrum is known as the visible spectrum.

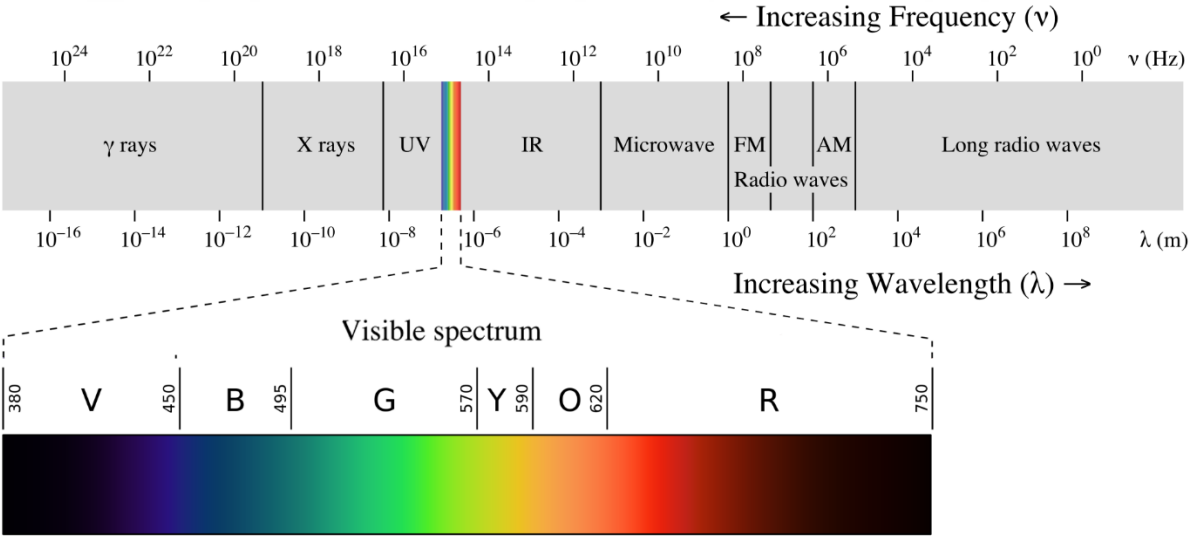


Figure 2.3 The Electromagnetic Spectrum.

At different bands of the electromagnetic spectrum are sensitive to the different types of land cover characteristics. The detection ranges of the electromagnetic spectrum are of great importance in the design of the sensors and in the selection of the satellite image to be used in a study. It is not possible to determine all the features of the earth with a single sensor. Different sensors are needed to detect chemical, thermal, electrical and physical properties in different regions of the electromagnetic spectrum (Musaoğlu 1999).

The earth’s atmosphere is transparent or partially transparent to a selected regions of electromagnetic energy.

Remote sensing images are composed of one or more bands. Each band contains values that represent the properties of LULC that is sensitive to. As well as the image can be formed by combination of multiple bands, images consisting of a single band are also available.

2.2. SPECTRAL RADIANCE PROPERTIES OF OBJECTS

The electromagnetic energy emitted by a natural or artificial source is reflected, absorbed or transmitted by the object it illuminates. The total incoming energy to the object is equal to the sum of the energies that are reflected, passed and absorbed by the body (Paine and Kiser 2012). Passed, reflected and absorbed radiation vary depending on the wavelength of the incident radiation and the physical properties of the object. The objects on earth can be distinguished from the differences in their spectral reflections.

The objects whose spectral reflectance differs clearly in certain spectral regions appear in different gray hues and colors in the remote sensing images sensitive to these regions. In this respect, the knowledge of the spectral reflectance properties of objects plays an important role in the spectral band selection.

2.2.1 Spectral Reflection of Plants

The cell structure (thickness, width), water content of the leaf and leaf pigments (chlorophyll, carotone, xanthophylls (yellow pigments), red pigment) act on the spectral reflection of plants. In the visible region, the leaf pigments absorb the radiation in red band and reduce the reflection. The chlorophyll reflects the radiation in near infrared band (Musaoğlu 1999).

In some plants, the reduction of chlorophyll in the leaves in autumn causes the caratones and xanthophylls (yellow pigments) to increase and the leaf appears yellow. If the red pigment increases with the reduction of chlorophyll in the plant, the leaf appears in light red. In the near-infrared region (0.40-1.30 μm), leaf pigments are completely permeable, because of the water content in the leaf only a small amount is swallowed at wavelengths of 0.98-1,20 μm . Since the spectral reflectivity in this region is closely related to the leaf structure, the health status of the plants can be distinguished from the differences in reflectance.

2.2.2 Spectral Reflection of Ground Surface

The composition of the top layer of the ground affects the spectral properties of reflected electromagnetic waves. The reflective properties of grounds depend on the water content of the ground, the type, structure, texture, surface roughness and the organic matter composition of the ground. As the water content in the soil increases, the reflection is reduced and the soil appear dark. In the absence of water on the soil, the structure of the ground becomes important. Soil with coarse textured appears darker due to an increase in surface roughness. Soils with higher content of organic matter also appears dark (Musaoğlu 1999).

2.2.3 Spectral Reflection of Water

The reflection of water varies depending on the state of the water surface, the suspended substances in the water, the base of the water, the organic matter in the water and the amount of chlorophyll. The turbidity of the water causes the reflection to increase. An increase in the amount of chlorophyll causes the reflection of water on the blue wavelength to decrease and the increase in the green wavelength. In the infrared region, since a large part of the incoming radiation is absorbed, the water appears dark (Musaoğlu 1999).

2.2.4 Spectral Radiation of Surface Bodies

The bodies on the earth do not merely reflect the incoming radiation, but emit the energy that they store in a wide spectral region as self-radiation. Each body heats up differently under the same radiation effect depending on its properties, and emits this heat in different amounts depending on its radiation coefficients. In thermal images, objects have different hue characteristics from photographic images, and hot surfaces are in a light color tone, cold surfaces appear in a dark tone.



CHAPTER 3

DIGITAL IMAGE PROCESSING TECHNIQUES

3.1 DIGITAL IMAGE

In the remote sensing system, the sensor senses the energy, measures and converts the amount to a number that the computer can read. The remote sensing spacecraft sends these codes to the ground station. These codes are converted to series of numbers. Rows and columns are represented by a number corresponding to a gray value and form a digital image (Figure 3.1). The smallest element of a digital image is called pixel.

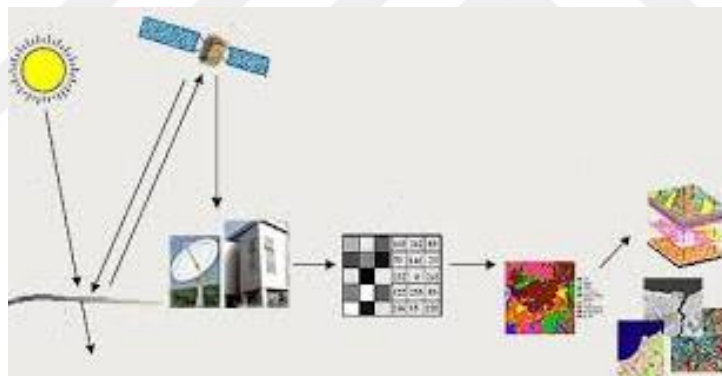


Figure 3.1 Elements of Digital Image.

In summary, the digital image is the numerical expression of the radiation vectors at different wavelength ranges. The average reflection value of the region corresponding to a small area on the earth is expressed by the numerical value corresponding to a pixel (Ekercin 2007).

Digital image is defined as a function of two simple variables. In a picture expressed by a function such as $f(a, x, y)$, where a is a unit of intensity and x and y are the actual coordinates of a pixel.

3.2 RESOLUTION OF A REMOTE SENSING IMAGE

Resolution can be defined as the number of pixels displayed in the image tool or the area of the earth represented by the pixel in the image file. Resolution refers to the distinguishing power of details. When the resolution of a satellite image is mentioned, there are four different resolutions which are spectral, spatial, radiometric and temporal.

3.2.1 Spectral Resolution

Spectral resolution is related to the width of the wavelength channels (Harrison and Jupp 1989). The detection range of a sensor in the electromagnetic spectrum is defined as spectral resolution. Sensing in different and narrow spectral ranges provides detailed information from the study area.

This term is used to define the wavelength measurement capacities of the sensors measuring the reflected energy. Wavelengths are expressed on a micrometer or micron scale. The number of bands is used to describe individual reflection wavelengths which can be measured by the system. For example; a quad band multispectral sensor measures the reflected energy at four different wavelengths. However, a multispectral image may consist of only 3 bands. Because, only three primary colors (red, green, blue) can be used to create a color image. Color images are created by combining red, green and blue bands, but this does not mean that we should not use reflection values of different wavelengths in these main bands. Normal RGB (red, green, blue) image can be described as the plants in green color while the sea in blue color. In order to create such an image, in a remote sensing software it is necessary to select the band corresponding to the red color wavelength of the image for the red band and the band corresponding to the green color wavelength of the image for the green band. The same procedure should be applied to the blue band. When this procedure is performed, a satellite image in normal colors is obtained.

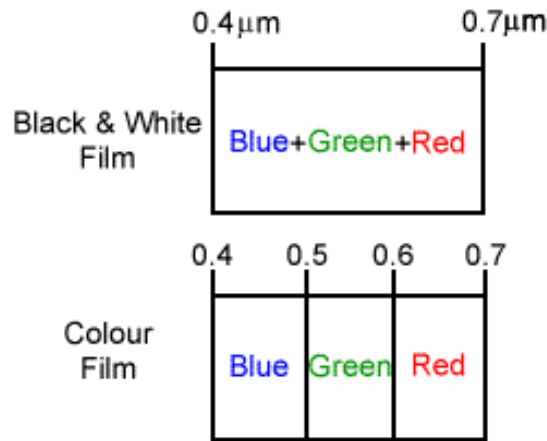


Figure 3.2 Natural Color Combinations.

However, in some cases different wavelengths can be defined for these three colors. For instance, if green, red and near infrared bands are selected for blue, green, and red colors respectively, green plants will appear in bright red in such a satellite image. This type of images are called as "false color" images. The pictures that shows how the natural color combination is obtained can be found in Figure 3.2.

3.2.2 Spatial Resolution

Spatial resolution is the spatial extend of pixel. The smaller the pixel size is, the greater is the spatial resolution (Figure 3.3). It is not easy to define the spatial resolution of an imaging system. The most common method used to determine spatial resolution is the IFOV (Instantaneous field of view), which depends on the geometric properties of the imaging system. Technically, it is the area where the sensor is displayed at a certain height (Mather and Koch 2011). It can be expressed as the smallest unit that the sensor can distinguish on earth. The spatial resolution is directly related to the scale of the map to be produced from the satellite image.

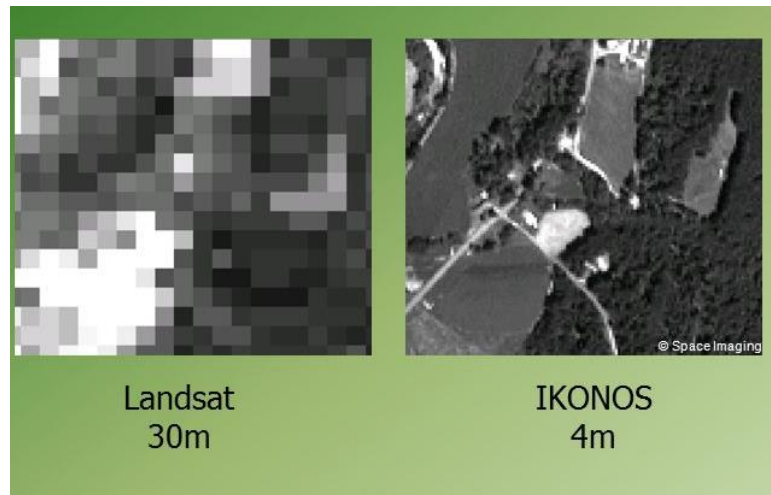
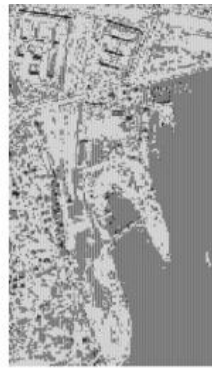


Figure 3.3 The spatial resolutions of the Landsat (30 m) vs. the IKONOS image (4 m).

The smallest object size you can define from the properties of the earth corresponds to the spatial resolution on an image. Spatial resolution is the most important feature to consider when making image selection. Because, taking the surface properties directly from the image can be examined depends on the spatial resolution. The dimensions of the objects planned to be investigated should be determined and then the image with the resolution having the ability to identify them and place them in the correct location should be selected. This is very important as it is directly related to the cost of your projects, because generally more detailed (high resolution) images are more expensive per unit area.

3.2.3 Radiometric Resolution

The radiometric resolution determines the sensitivity to the amount of electromagnetic energy in the image taken by a sensor. It is the ability to determine very small changes in electromagnetic energy (Duran 2007). Figure 3.4 shows a sample of images with different radiometric resolution. Modern remote sensing instruments have usually 16 bit radiometric resolution. This means that each pixel can take one of 65536 possible values.



**2-bit
4 gray levels**



**8-bit
256 gray levels**

Figure 3.4 Radiometric resolution sample.

3.2.4 Temporal Resolution

Temporal resolution is expressed as the shortest time that a sensor is able to revisit the same area of the earth. Especially, the temporal resolution of the sensor is important in change analyzes.

The physical properties of objects on earth will be subjected to a number of changes within the optimal time intervals at which these properties can be observed. The appropriate time interval can be years, seasons, days or weeks. For some applications, time interval is an even more important factor in remote sensing results. For example, following product growth and development, it is of great importance to obtain images at predetermined short time intervals. However, in an effort to investigate the development of a settlement, this may be a period of one year or more.

3.3 IMAGE CLASSIFICATION

Image classification is a process of assigning a land cover type or class to each pixels in the image. Image classification is is a decision making process.

Various analysis and interpretation techniques are used in order to get information from the satellite images. One of the most common ways to convert data into information is the classification of satellite images. The classification in remote sensing creates combinations with different values in the digital image depending on the different natural spectral reflection and

spreading properties of the objects. By using this difference, objects on earth can be grouped with the same spectral characteristics. In the database language, the property space is divided into independent regions that allow for a multiple-to-one relationship between objects and classes. As a result, each object is included in a definite class or not included in any class (Karakış 2005). It can be seen as a decision making process used in branches of science where remote sensing is integrated.

The image obtained as a result of classification is called the thematic map. The image classified as a thematic map can be used in geographic information systems (Jehnsen 1996). In the classification process, the creation of the classes depends on the purpose and scale of the work to be carried out. The classification process is divided into two main groups as pixel-based and object-based classification.

3.3.1 Pixel-Based Classification

The processing unit of the pixel-based classification approach is pixel. Here, the spectral value of pixels and the neighboring relations between pixels are handled. They are two methods to perform pixel-based classification. They are the unsupervised and supervised method.

3.3.1.1 Supervised Classification

Supervised classification is performed based on external data of the areas on the image. The requested classes are created by the user. In this method, it is predetermined to select which classes are desired from the image, by selecting samples or defining class properties. The choice of control areas is a stage that affects classification. The common problem in the application is class conflict. Class conflict usually results from measurement of control areas. Therefore, class defining must be very sensitive, but this is almost impossible. It is aimed that the class to be defined is assigned to the maximum similar class based on the calculated probability value.

Three approaches are used in the supervised classification process.

- Maximum likelihood
- Paralel lepiped
- Minimum distance

3.3.1.1.1 Maximum likelihood method

It is the most widely used algorithm of supervised classification. This method takes into account the accurate estimation of the average values and covariance matrix for each spectral class. The functions for the classes that make up the control areas are calculated and it is decided which class is closer to a pixel. At this stage, the user determines that the threshold value is used to determine whether the pixel to be classified is in a class other than the specified classes or class (Çölkesen 2009). When there is not enough data in the sampling area (when there is no data to accurately estimate the probability distributions of the classes), the desired classification accuracy cannot be reached. In this case, other classification methods that do not use covariance information should be consulted.

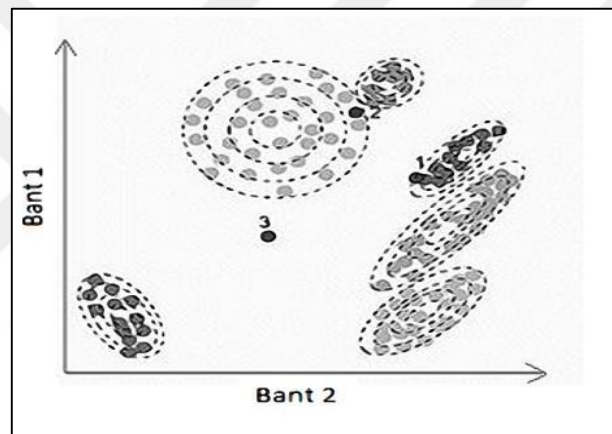


Figure 3.5 Illustration of the maximum likelihood method.

3.3.1.1.2 Paralel lepiped method

In terms of calculation time, this method is quick and simple for mathematical expression. It is based on the examination of the histograms of spectral components of the sampling (control) data. Rectangular regions are created, taking into account the minimum and maximum spectral values in the band for each sample class. Then, the candidate to be classified is assigned to the class to which the rectangular region belongs (Lillesand et. al. 2007). The number of pixels not classified in this method is high so, the classification process becomes difficult. The problem is solved by randomly assigning candidate pixels to one of the overlapping classes.

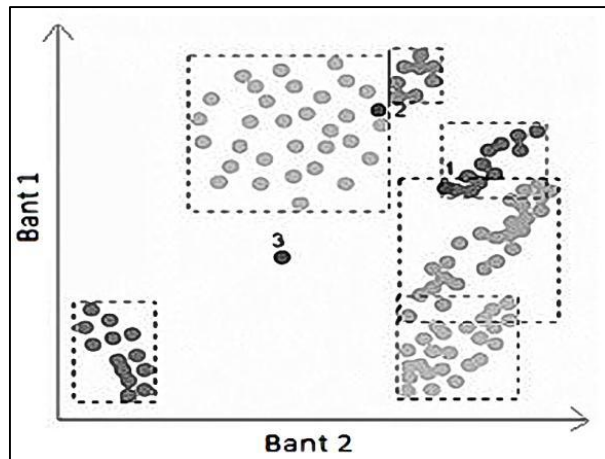


Figure 3.6 Illustration of the paralel lepiped method.

3.3.1.1.3 Minimum distance method

The candidate pixels are assigned to the sample class at the shortest distance according to the calculated spectral distances between the average vector and candidate pixels calculated for each sample class. It is an easy and fast algorithm for calculation. It is advantageous because it is faster than the maximum likelihood method. The class models are spectrally symmetrical, because covariance information is not used.

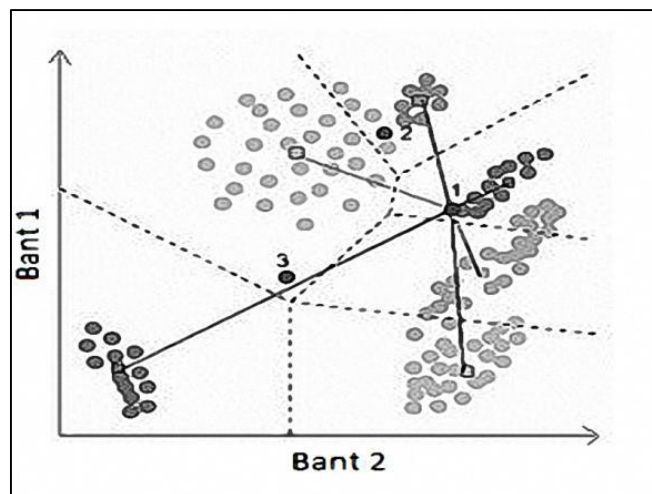


Figure 3.7 Minimum distance classifier.

3.2.1.2 Unsupervised Classification

It is used in studies where there is not enough information about the study area and pre-knowledge is needed about the general structure of the region. The characteristics of the classes

are determined by comparing the aerial photographs of the region, topographic maps and existing information. Minimum distance is used as decision rule. Pixels are analyzed from left to right and line by line by starting at the top left corner of the image. The spectral distance between the candidate pixels and the mean of each cluster is calculated and assigned to the nearest cluster. Cluster centers are temporarily calculated to determine the pixels that will be included in classes, and this process continues until there is no change in the positions of cluster centers.

The big disadvantage is that the classification can lead to repeating numerous times. In contrast, the ability to fully and systematically analyze the statistics of objects is the advantage of unsupervised classification. Thus, the results of an unsupervised classification can give useful information about the classes that can be detected. However, it is often possible to formulate uncertainties, depending on the classification parameters, not depending on classes and their characteristics.

3.3.2 Object-Based Classification

Classical pixel-based approaches have a wide range of uses, but operations on the spatial scale of the pixel can cause many shortcomings. This is because the spatial width of a pixel may not match the vegetation of the relevant feature. For example, what a pixel represents more than a single type of vegetation is known as the problem of mixed pixels (Aplin and Smith 2008). Classic pixel-based classification approaches are not sufficiently suitable for high spatial resolution images (Schiewe et. al. 2001). Object-based image analysis provides an advantage over traditional methods because it is a method that evaluates objects according to different criteria such as color and shape, integrity, texture properties, neighbor relations by analyzing close to human perception (Uça Avcı ve Sunar 2010).

Here, since object-based image analysis is used to group objects with similar spectral properties, the smallest unit is the object, not the pixel. The processing of features within the image by grouping them into objects forms the basis for object-based image analysis. This approach allows the image to be analyzed in close proximity to human perception. In an object-based approach, objects form the basis of images, photographs, or image formats. For example, when looked at a photograph, shape, text, color, content and other features that can be understood in the picture are used, and the image is analyzed by dividing into various objects. The human brain has an innate ability to interpret the rich information content that exists in a picture, and

can intuitively identify objects of other characteristics such as cars, houses, trees, golf courses. In other words, the power of reasoning allows the sudden use of previously stored information in the human brain and transforms it into a specialized rule base for image interpretation.

Objects are created by combining homogeneous neighboring pixels in the segmentation which is the first process step of the object-based image analysis. The next process from segmentation is classification. Morphological characteristics of these objects obtained in the classification are utilized. One of the advantages of this analysis is that, instead of dealing with millions of pixels, using a small number of homogeneous integrated objects created in the segmentation.

Image classification is the most commonly used method for extracting information about earth objects with the help of remotely sensed images. In today's image processing techniques, object based classification method is used instead of traditional pixel based classification method. The most important reason for this is the increase of the spatial resolutions of satellite image data and aerial photographs in recent years and the fact that the rich information content available cannot be fully revealed as a result of pixel-based classification approaches. In classic pixel-based classifications, it is only essential to extract detail based on the gray value of the pixel. High resolution data can yield inconsistent results in pixel-based classification results due to rich information content.

Object-based classification is an inverse approach to traditional pixel and sub-pixel based classification, based on grouping pixels with similar spectral properties on the image, creating image objects representing these pixels, and classifying the objects instead of pixels (Blaschke 2010, Myint et. al. 2011). This process classifies objects representing them rather than millions of pixels on the image. A large number of additional information can be extracted from image objects. The information from the shape, texture, neighborhood and other object layers is the source of this. Most of this information is specific to the object-based classification method. The more accurate classification results can be obtained by using the attributes of the object. According to the object-based classification approach, an object (segment) is defined as a group of pixels with similar spectral and spatial characteristics (Altunkaya ve Yastıklı 2011). This type of segmentation and topology formation should be adjusted according to the resolution and scale of the objects. Image information can be presented at different scales depending on the average size of the image objects. The same image can be segmented as smaller or larger objects. In this case, it can greatly affect all information derived from image objects. Therefore,

different information can be extracted from each scale. It is possible to present this information in different object layers simultaneously as image information on a different scale. It can contribute to the extraction of many additional information by associating the object layers in this structure with each other (Marangoz et. al. 2005).

The characteristic of the object-based approach is the cyclic interaction between the processing and classification of image objects. Depending on the segmentation, scale, and the shape of the image objects, specific information is available for classification. Conversely, special algorithm operations can be activated depending on the classification. In most applications, the desired geographic information and objects of interest can be obtained step by step with the iterative cycle of classification and processing. Thus, the shapes, class assignments, and interrelationships of image objects which are the processing units are constantly changed (Karakış 2005).



CHAPTER 4

DATA AND METHODS

4.1 STUDY AREA

Gemlik was selected as a study area because of it is diversified in terms of land cover and land use, agricultural areas and forest areas. Gemlik is a municipality of Bursa district, Republic of Turkey located on the shores of the Marmara Sea. Gemlik is surrounded by mountain ranges and to the West it borders the Sea of Marmara.

The Gemlik municipality is located approximately 30 km north of Bursa. Upper left and lower right geographical coordinates of study area are 40.46°N, 29.06°E and 40.37°N, 29.20°E, respectively. The slopes of the mountain ranges and plains surrounding the Gulf of Gemlik form the territory of the municipality. The biggest plains are the Engürücük and Gemlik. The municipality center is located at the western fringes of Gemlik plain. The total area of the Gemlik municipality is 376 km². The terrain elevation reaches up to 1283 m in the Katırlı Mountains. The AOI is drained by the Karsak river with its tributaries discharging its waters to the Gulf of Gemlik. Figure 4.1 shows the location of the study area (or the Area of Interest abbreviated as AOI).



Figure 4.1 Topography of AOI, Gemlik.

The Gemlik municipality is under influence of the Mediterranean climate. Summers are hot and winters are cold occasionally with subzero temperatures. The AOI receives the majority of its precipitation during winter months (December to April). In the past the area was frequently snow covered, although in recent years snow cover is rare phenomenon. The daily average precipitation data for 2017 are shown in Figure 4.2.

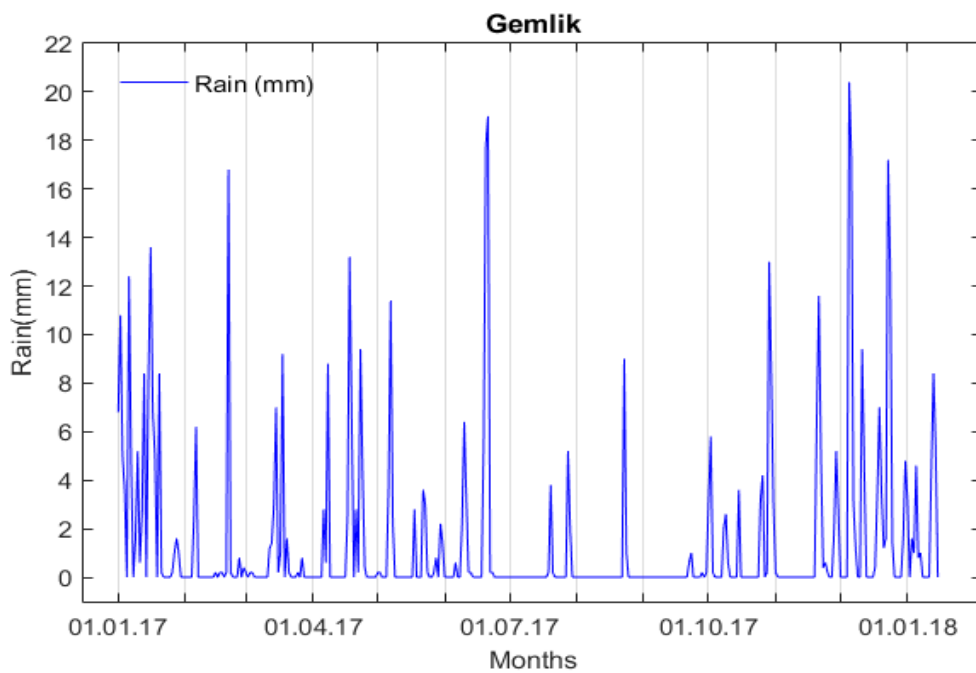


Figure 4.2 Daily parameter of rain at 2017 in Gemlik.

The daily average temperature for 2017 is as shown in Figure 4.3.

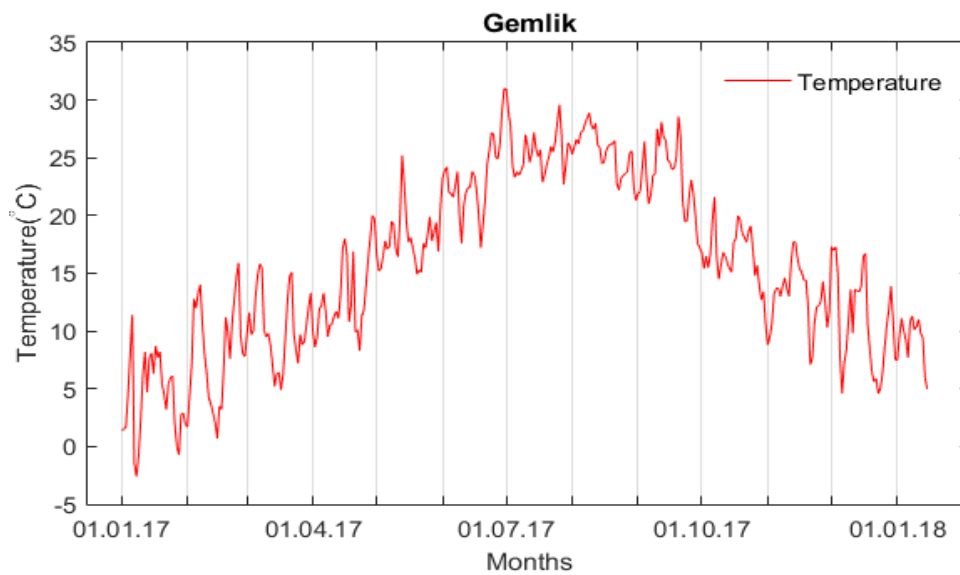


Figure 4.3 Daily parameter of temperature at 2017 in Gemlik.

Effects of climate

- 1) Depending on the climate, maquis is seen on the shores of the Marmara Sea, while large and coniferous forest on the high levels.
- 2) The rivers carry most of the water in winter and spring, while the least water in the summer.
- 3) the climate conditions are different and not so hard, leads to an increase in population density
- 4) The existence of three climate types increased the productivity on the plains and diversified agricultural products.
- 5) The region is suitable for growing industrial plants (sugar beet, olive, corn, cereals, vegetables and fruits)
- 6) Region is rich in forest.

Vegetation Cover

The population of the city is 103390 according to the 2014 National Census. Gemlik, is the port of Bursa. The agricultural products in the region have a great importance in the trade, which is the source of livelihood of the people. 80% of the population living in Gemlik municipality is engaged in trade. Salted olive and olive oil are the leading commodities. Agriculture in Gemlik

is well developed. Olive production is mostly preferred. It is one of the places where the most delicious table olives are grown in Turkey. High quality apples, pears and peaches are also produced. Turkey's first canning factory was established there, due to the development of conservation, production of vegetables have been developed. Beans, artichokes, cucumbers, tomatoes, peas, eggplant and pepper come at the beginning of the vegetables. When we evaluate the scope of agricultural areas, the distribution of agricultural areas in Gemlik region is about as given in Table 4.1.

Table 4.1 Distribution of agricultural land usage in Gemlik.

Agricultural area	Year	Decare	Percentage
Fruits Beverage and Spice Plants	2017	83660	80.17
Fallowing	2017	5615	5.38
Vegetables	2017	1460	1.40
Cereals And Other Herbal Products	2017	13618	13.05
Total	2017	104353	100.00

As seen in Table 4.1, it has a large proportion used for fruits beverage and spice plants. The products types grown in agricultural areas used for fruit beverage and spice plants are shown in Table 4.2.

As it seen in Table 4.2, the most important part of the agricultural areas with the land covering 82000 decare are olive orchards. These olive groves provide significant contributions to the local people with the production of table olives and olive oil.

Table 4.2 Product types of Fruit and Spice Plants in Gemlik.

Fruits Beverage and Spice Plants	Year	Decare	Percentage
Fig	2017	10	0.01
Apple (Golden)	2017	10	0.01
Apple (Starking)	2017	141	0.17
Apple(Other)	2017	20	0.02
Pear	2017	20	0.02
Quince	2017	90	0.11
Cherry	2017	161	0.19
Sour cherry	2017	2	0.00
Peach	2017	1316	1.57
Nectarine	2017	10	0.01
Plum	2017	10	0.01
Hazelnut	2017	90	0.11
Walnut	2017	19	0.02
Olive	2017	81761	97.73
Total	2017	83660	100.00

When the vegetables are handled, as shown in Table 4.3.

Table 4.3 Product types of Vegetables in Gemlik.

Vegetables	Year	Decare	Percentage
Green beans	2017	400	27.40
Black cabbage	2017	20	1.37
Lettuce	2017	50	3.42
Artichoke	2017	200	13.70
Parsley	2017	10	0.68
Water melon	2017	50	3.42
Bell pepper	2017	40	2.74
Long green pepper	2017	90	6.16
Cucumber	2017	80	5.48
Eggplant	2017	160	10.96
Tomato	2017	350	23.97
Onion	2017	10	0.68
Total	2017	1460	100.00

While green beans and tomatoes are widely grown vegetables, artichoke and eggplant follows them. The region is also known for its peach production. If we consider the production of cereals, as shown in Table 4.4.

Table 4.4 shows that wheat and barley production is widely used. While the wheat produced here is used for bakery products, barley is used for cooking or beer production.

Table 4.4 Product types in Cereals And Other Herbal Products in Gemlik, 2017.

Cereals And Other Herbal Products	Year	Decare	Percentage
Wheat berry	2017	10339	75.92
Corn	2017	577	4.24
Barley	2017	1848	13.57
Oat	2017	586	4.30
Clover	2017	268	1.97
Total	2017	13618	100.00

Olive production in Gemlik industry holds a large place. The Sumerbank Suni Silk Factory, which was established in 1937, played an important role in the development of the district. Tügsaş (production of fertilizers and chemical products), Borusan (pipe production), Çimtaş (production of steel and iron), Borçelik (steel production) and MKS (chemical industry) are the basis of the industry in Gemlik.

Summary of the geography of AOI

- 1) Only mountainous areas are covered by forest. No forest cover is present at lower elevations of the AOI. In total the forest covers approximately 40% of AOI.
- 2) Rivers discharge most of the water during winter and spring months, the climate conditions are mild and therefore preferred by farmers.
- 3) The region is suitable for growing industrial plants (sugar beet, olive, corn, cereals, vegetables and fruits).

4.2 DATA

The Sentinel-2A/B images to be used in this study. They are available free of charge from the Copernicus Open Access Hub program. The Sentinel 2A/B imagery for January 2017 to January 2018 were acquired from the hub. The first Sentinel 2A/B image belonging to each month was requested to be used in the image selection of the region in order to observe the time-dependent change. However, due to the influence of cloudiness in the regions containing the study area on the images, this selection could not be carried out regularly. Therefore, the first image without a cloud is used for each month.

4.2.1 NDVI

There are a number of different vegetation indexes which are designed to assess the vegetation status and monitor its change. The most common index is the Normalized Difference Vegetation Index (NDVI). Despite of the progress of agricultural techniques, climatic factors continue significantly affect agricultural production. The NDVI index calculated from the multispectral satellite imagery is one of the ways to show the impact of climatic conditions on vegetation. As the amount of rain increases, the vegetation viability also increases, which leads to an increase in the value of NDVI. And the higher NDVI values indicate that the yield of the monitored crops will also increase or vice versa.

In summary, NDVI is a scale ranging from 1, which indicates the presence of healthy vegetation and -1, indicating no vegetation. In general, healthy plants are green and the unhealthy ones are brown. In this study, NDVI was selected to assess the land cover change over time. The following is the data processing steps used in this project. Firstly, B4 (Red) and B8 (NIR) bands are opened in ArcGIS program and our selection region is clipped. The NDVI was calculated from the clipped bands and this process was repeated for each month's image as shown in Figure 4.4. The NDVI is calculated using the Raster Calculator tool from band B8 and B4 as follows:

$$NDVI = \frac{B8 - B4}{B8 + B4} \quad (4.1)$$

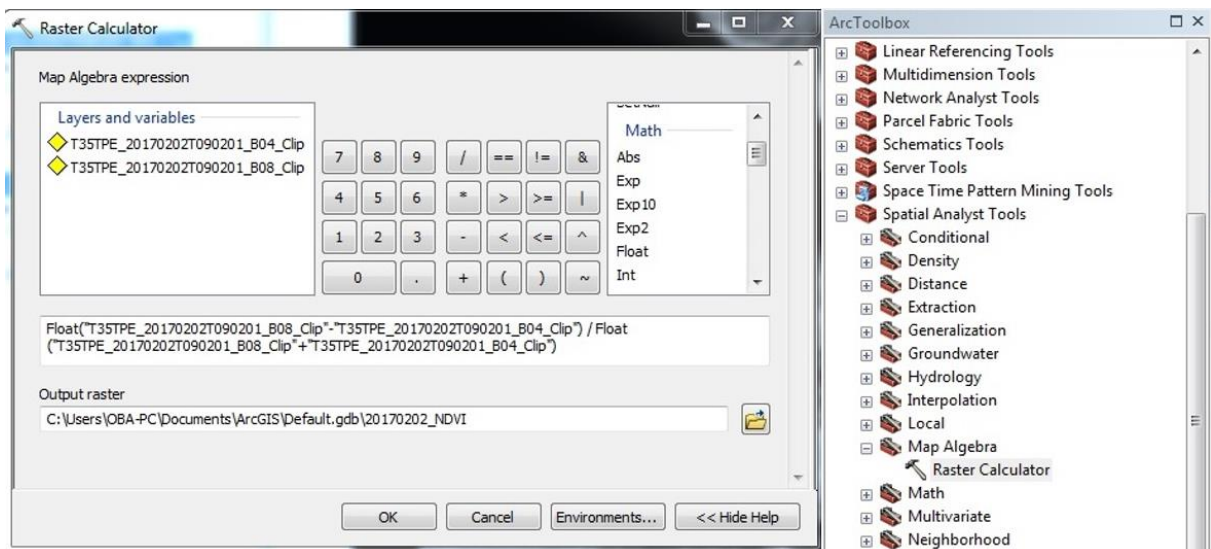


Figure 4.4 Calculation of NDVI imagery with ArcGIS.

4.2.2 Data Analysis Steps

After calculating the NDVI for each image, 13 NDVI images were used to create a single multi-band image. This image was subsequently used to observe land use changes over time by assigning to the RGB channel bands of interest from the composite image. For example, Figure 4.5 shows an image composed of the Red, Green and Blue channels to which the January, April and July 2017 were assigned, respectively.

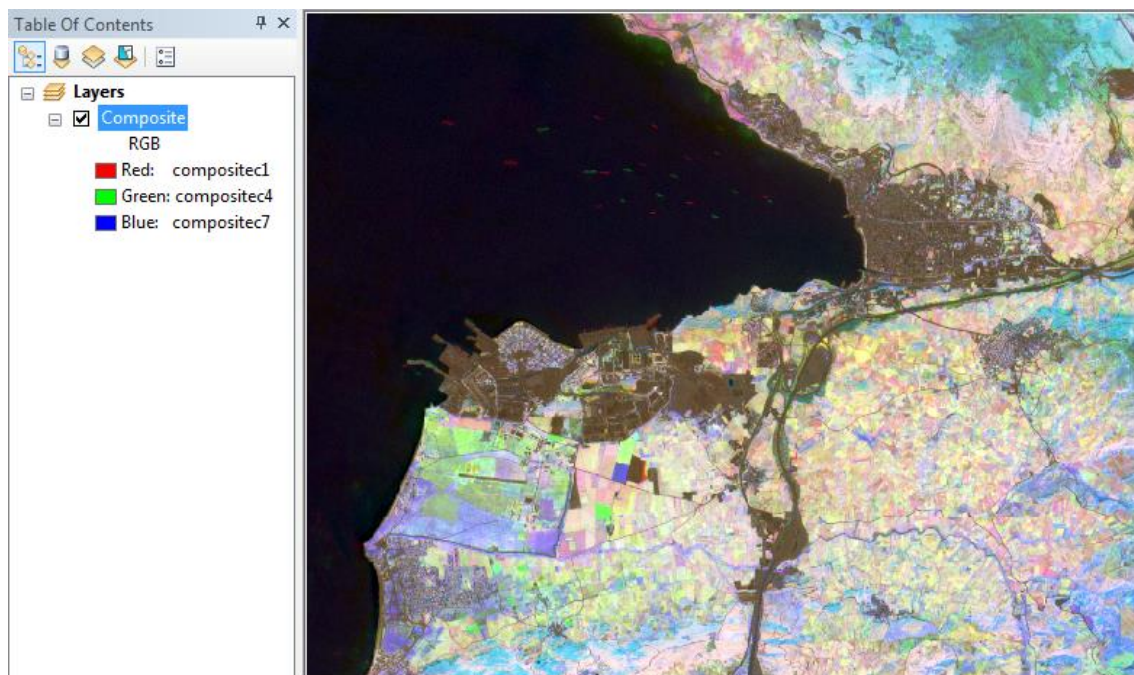


Figure 4.5 Composite image.

After calculating the NDVI values for each image, True (Natural) color images were created in order to improve photo interpretation task. To obtain natural color images, B4 (red), B3 (green) and B2 (blue) bands were opened in ArcGIS software, clipped to work area and created composites (Figure 4.6).

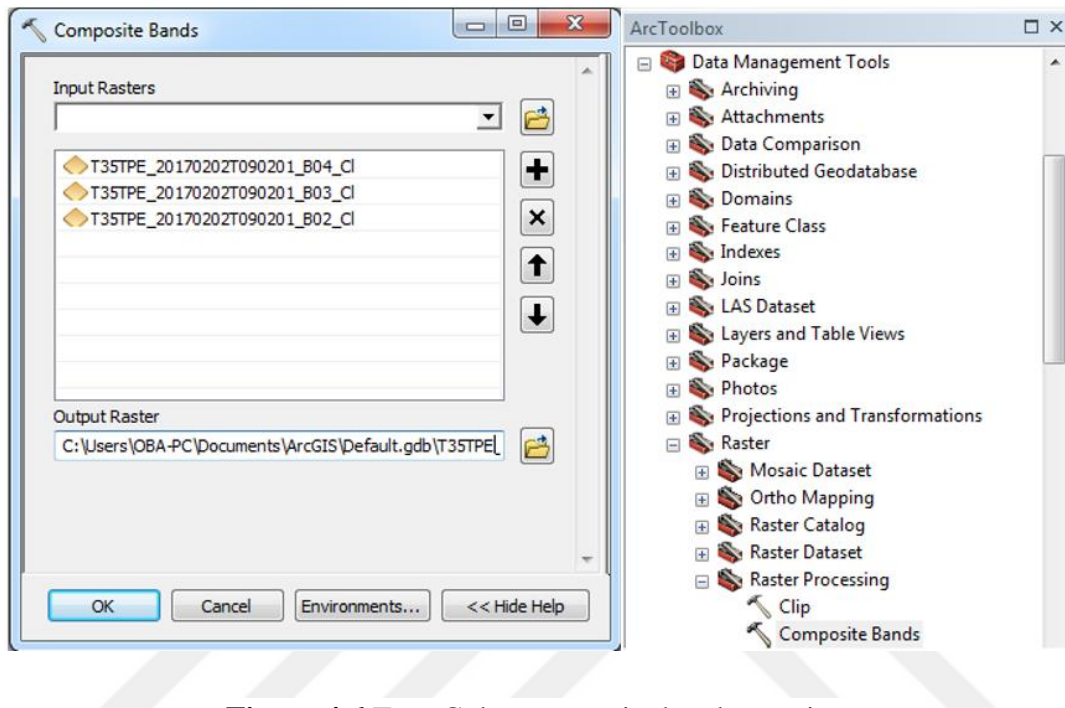


Figure 4.6 True Color composite bands creation.

Using the natural color image a test regions and lines representing sea, forest, agricultural, industrial urban and roads land use types were selected. Figure 4.7 to Figure 4.9 illustrate the above process.

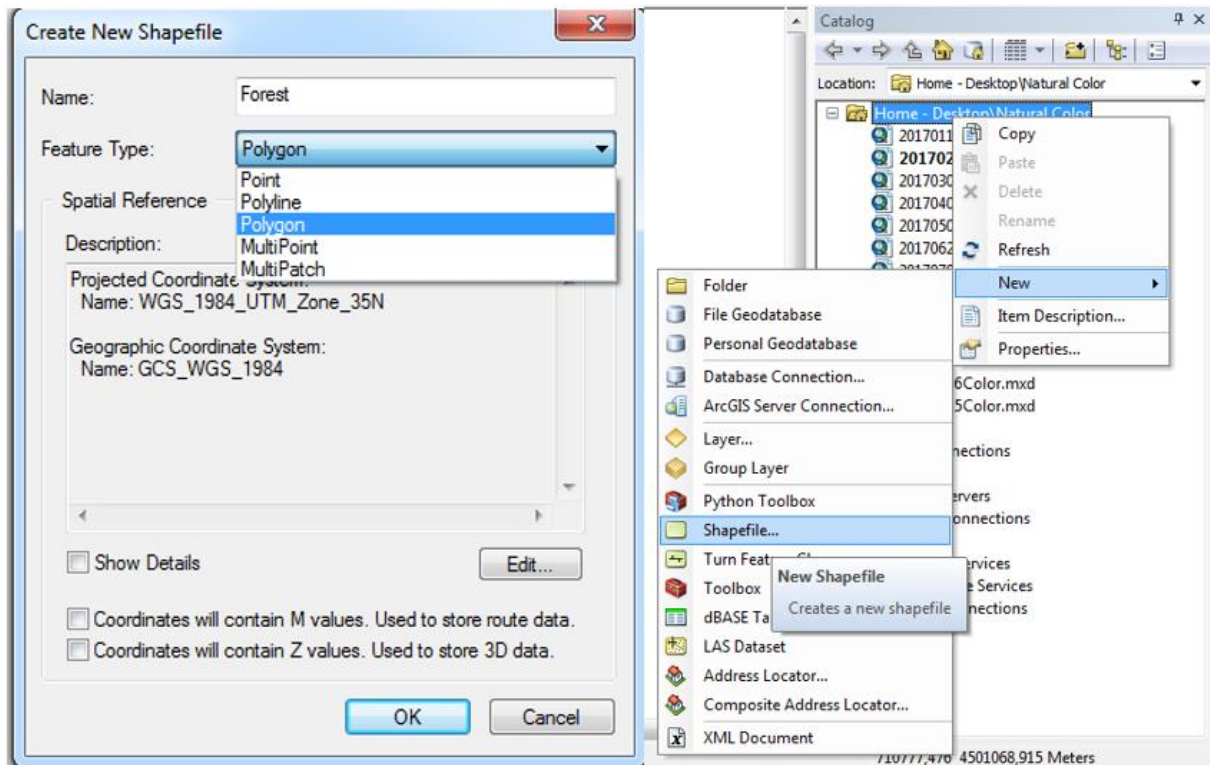


Figure 4.7 Defining the land cover types in ArcGIS.



Figure 4.8 Polygon selection of shapefiles.

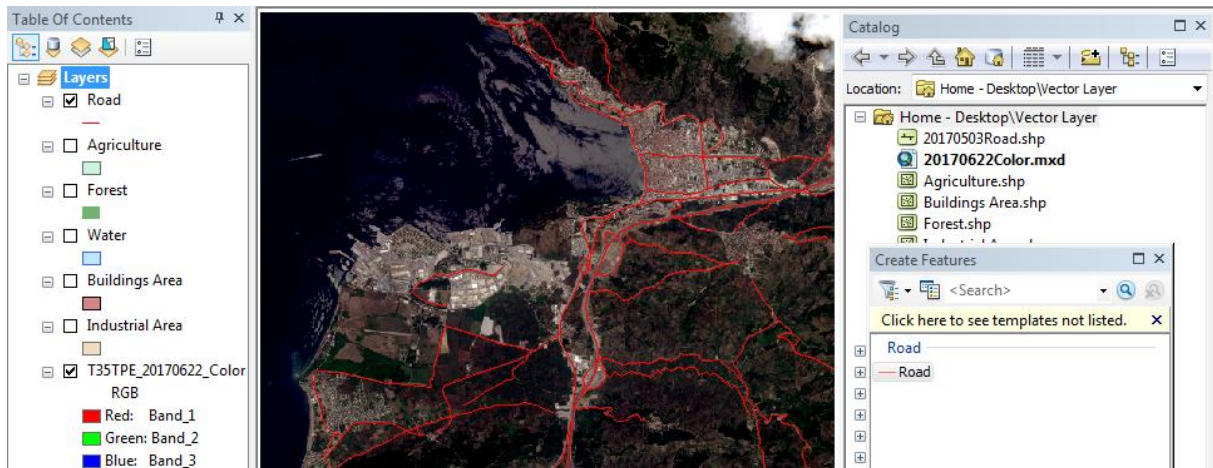


Figure 4.9 Polyline selection of shapefiles.

The statistics of the NDVI images for the selected polygons and lines were calculated after converting the, NDVI images to points, which is shown in Figure 4.10.

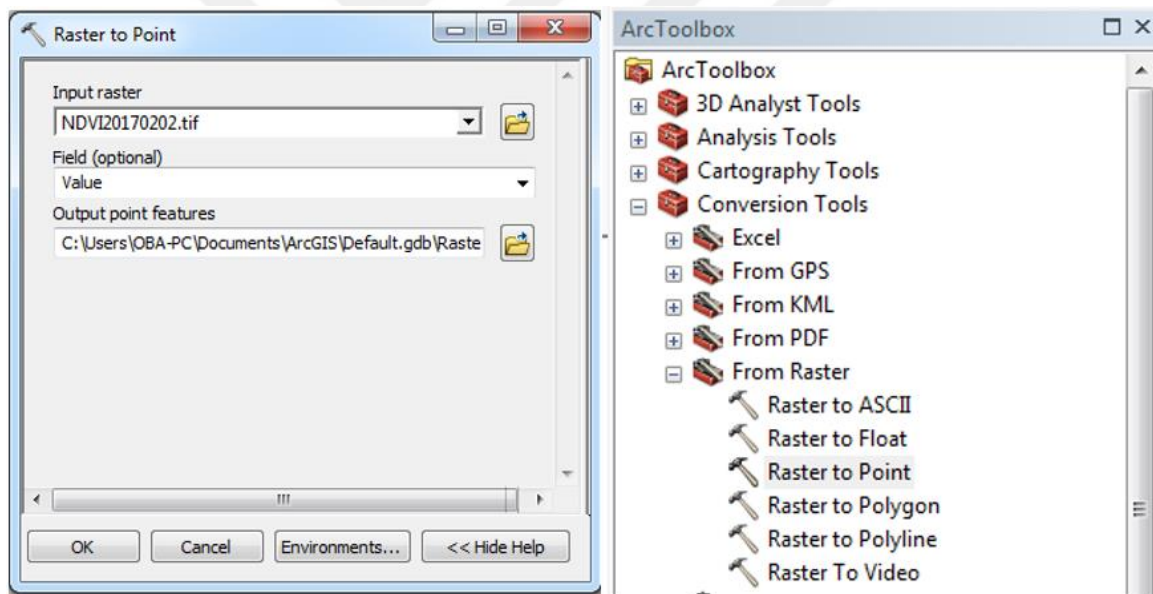


Figure 4.10 Raster to point conversion.

The NDVI points were joined with selected test regions for land cover class. This operation allowed for assigning to the select polygon and polylines the NDVI values and their statistics. To obtain a single statistic for each class, multiple polygons were combined using union and merge operations, and lines with dissolve operations as shown in Figure 4.11 and Figure 4.12.

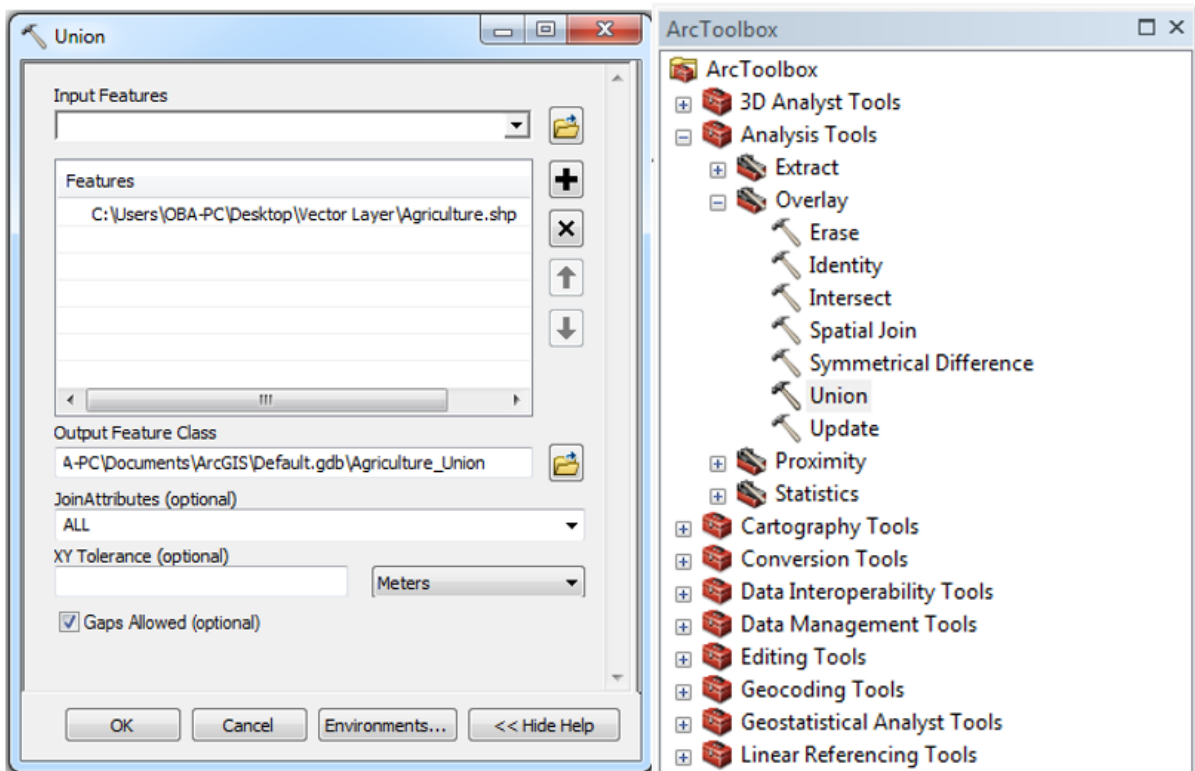


Figure 4.11 Creating polygon features union.

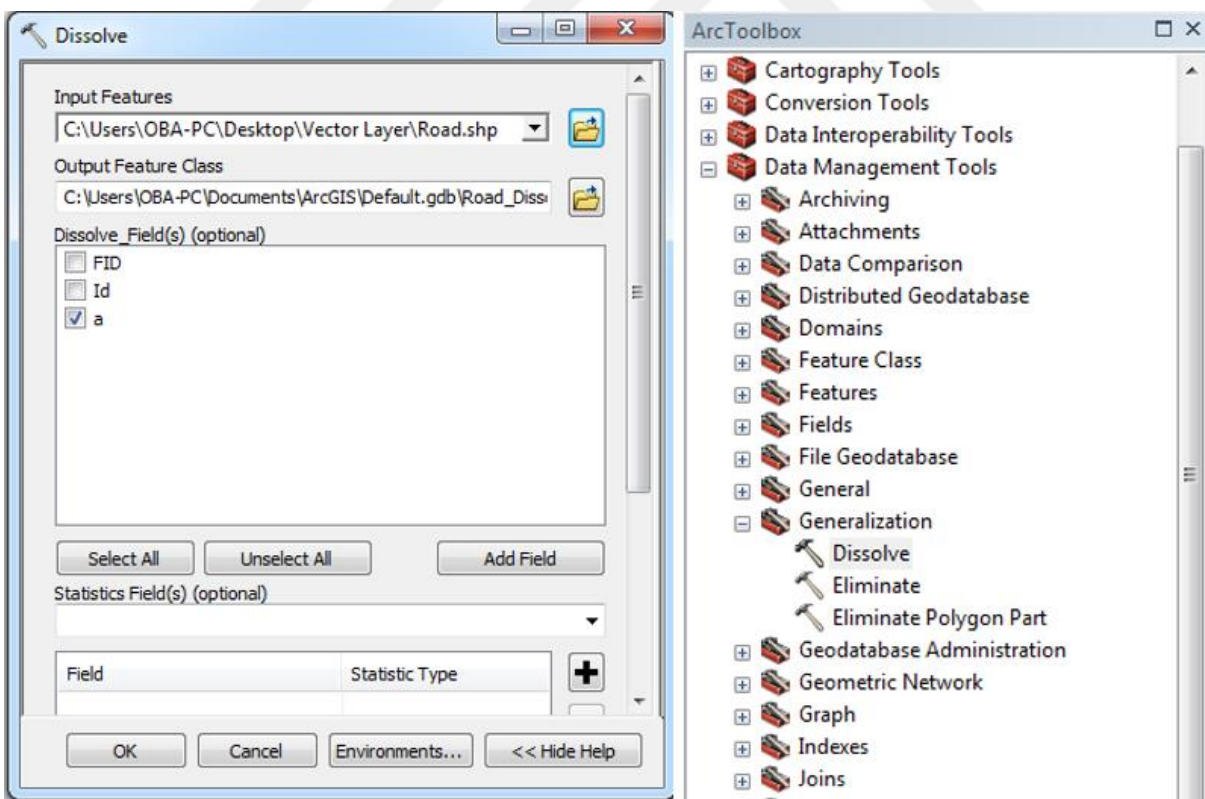


Figure 4.12 Creating polyline features dissolve.

Then, point data was joined to the shapefile of each class. This operation was repeated for 13 images as shown in Figure 4.13. During this operation, requested attributes like average, minimum, maximum and standard deviation options are selected in the opening window.

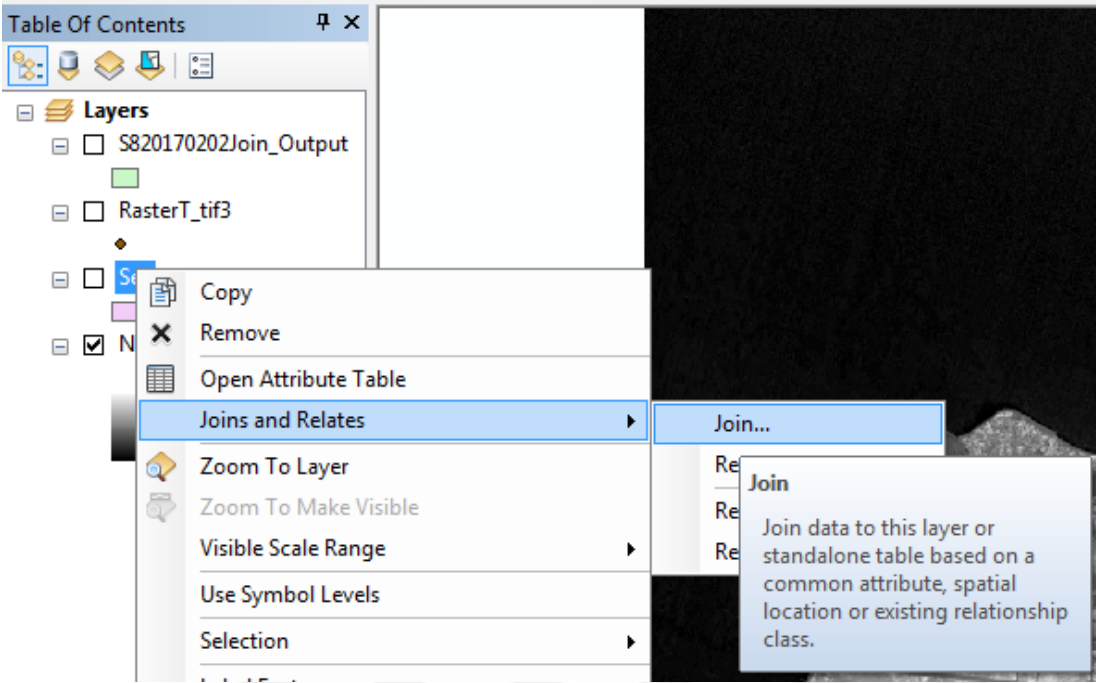


Figure 4.13 Point data join to the shapefiles.

Resulting table containing calculated statistics for each land cover class can be access as shown in Figure 4.14.

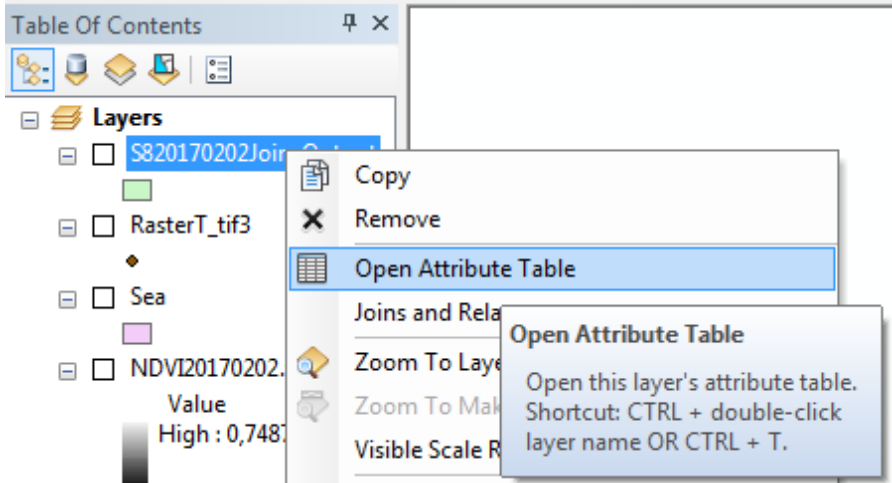


Figure 4.14 Open attribute table.

OBJECTID*	Shape*	Avg grid code	Min grid code	Max grid code	SD grid code
1	Polygon	-0,274533	-0,357834	0,28757	0,018674

Figure 4.15 Attribute table data sample for Sea, Feb 2017.

As it shown in Figure 4.15, statistics for points belonging to one of the selected test polygons are listed. The values in this table are for points staying only in the area created for the sea. Considering the evaluation of monthly images, this process will be repeated for 13 images from January 2017 to January 2018. After these operations, a 13-line attribute table will be obtained for each class as shown in Table 4.5.

Table 4.5 Monthly attribute table of Sea.

Date	Avg_grid_code	Min_grid_code	Max_grid_code	SD_grid_code
20170113	-0,3160	-0,4851	0,3109	0,0234
20170202	-0,2745	-0,3578	0,2876	0,0187
20170301	-0,2160	-0,2779	0,3837	0,0142
20170403	-0,2023	-0,2658	0,2225	0,0154
20170503	-0,1196	-0,1857	0,1754	0,0138
20170622	-0,2044	-0,4662	0,2359	0,0358
20170702	-0,0748	-0,2721	0,2821	0,0187
20170813	-0,2625	-0,3360	0,2437	0,0196
20170907	-0,2565	-0,4269	0,3497	0,0248
20171017	-0,2901	-0,5062	0,4980	0,0258
20171116	-0,2251	-0,2888	0,1952	0,0161
20171216	-0,2779	-0,4121	0,2426	0,0232
20180115	-0,2961	-0,3985	0,3112	0,0239

CHAPTER 5

RESULTS AND DISCUSSION

5.1 RESULTS

Quantitative land cover and land use change analysis is the method based on geometrically corrected a time series of remote sensing imagery (Ramachandra and Kumar 2004).

In this chapter, the obtained results of the analysis of a time series of the NDVI index are outlined and subsequently discussed. The time series of the NDVI was developed based on 13 Sentinel 2 multi spectral images, and six arbitrary selected land cover classes. The selected land use classes were marked by polygons/polylines as a result of a photointerpretation of the natural colour composite images produced from three bands (R=4, G=3, B=2) of the Sentinel 2 images. For each polygon/polyline basic statistics of the NDVI, including mean, standard deviation and the range were calculated. The calculations were performed in the ArcGIS/ArcMap environment.

5.1.1 NDVI Results of the Road Type Land Cover Class

The spatial resolution of the B2 (Blue), B3 (Green), B4 (Red) and B8 (Near Infrared) bands of Sentinel 2 satellite images is 10 m. The width of the Roads Class selected for the study vary between 5 m and 36 m. Therefore, some of the pixels for the narrower roads represent not only the surface of road, but also land cover material neighbouring the road itself.

Table 5.1 Attribute table of Road type class

Date	Avg.	Min	Max	SD
20170113	0.11	-0.84	1.00	0.33
20170202	0.15	-0.73	0.75	0.32
20170301	0.15	-0.60	0.70	0.27
20170403	0.20	-0.29	0.78	0.30
20170503	0.24	-0.19	0.73	0.27
20170622	0.21	-0.49	0.78	0.31
20170702	0.26	-0.33	0.86	0.28
20170813	0.17	-0.38	0.80	0.32
20170907	0.17	-0.44	0.79	0.32
20171017	0.18	-0.55	0.82	0.35
20171116	0.15	-0.45	0.73	0.28
20171216	0.18	-0.63	1.00	0.35
20180115	0.18	-1.00	1.00	0.36

Table 5.1 shows calculated statistics for NDVI index for the Road class. Overall the mean NDVI index during the entire time frame varies from 0.11 to 0.26 taking the lowest value in January and the highest one in July, 2017, respectively. It is suspected that the culmination of the NDVI during July is related to the mixed pixels contaminated with vegetation (higher value of NDVI).

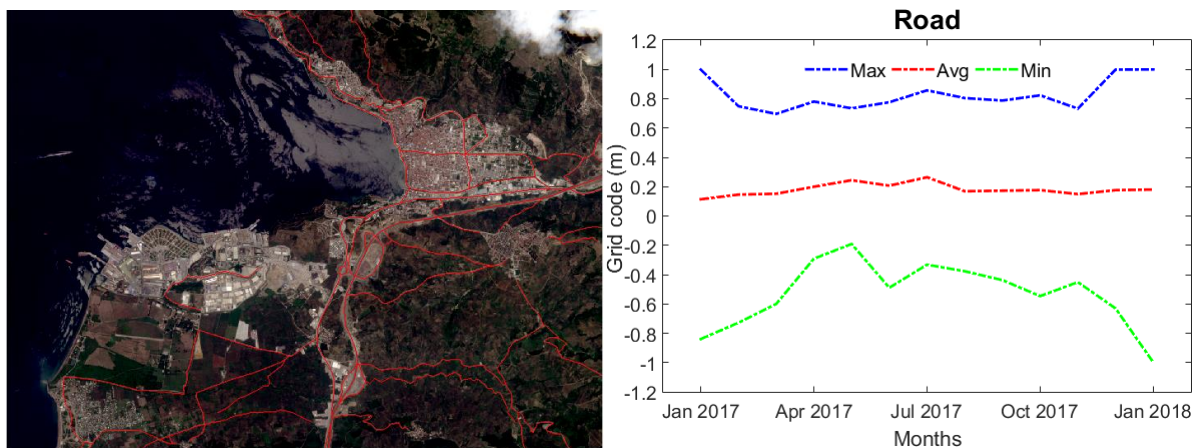


Figure 5.1 Time series of NDVI for the Road type class.

Since the routes we selected for the road class were different types such as asphalt, surface treatment and unpaved road, the standard deviation was high to approximately 0.3. Time series results of road class are illustrated in Figure 5.1.

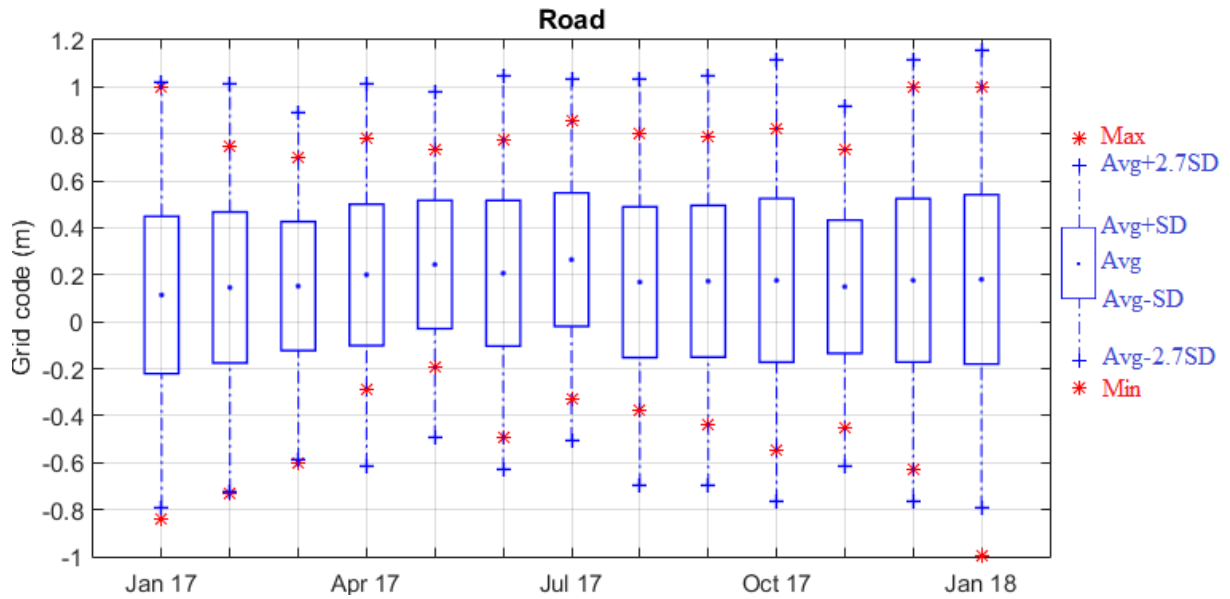


Figure 5.2 Standard deviation (SD) time series analysis of NDVI for the Road type class.

The minimum and maximum NDVI values are spread in the range of -1 to +1 due to the different types of road and different types of objects on the selected route. The 2.7 sigma confidence interval in this distribution for the road class is as shown in next figure. In Figure 5.2, “*” refers to the minimum and maximum values of the month and the rectangles shows the standard deviation, while “+” indicating the $\pm 2.7SD$.

5.1.2 NDVI Results of the Industrial Area Type Land Cover Class

The Bursa Free Zone, which is located in the border of Gemlik, is one of the 20 free industrial zones in Turkey. These free zones are the regions within the country where, the custom, tax and other regulations are significantly relaxed. The Bursa Free Zone is the sixth in the trade volume in all Free Zones with a volume of USD 1,766,081,782 in trade volume in 2007. In terms of employment, it holds the second place with an employment volume of 10,073 people. The Bursa Free Zone's contribution to Gemlik's economy and employment is significant.

Table 5.2 Attribute table of Industrial Area type land cover class.

Date	Avg.	Min	Max	SD
20170113	0.06	-0.22	0.56	0.10
20170202	0.06	-0.19	0.51	0.09
20170301	0.06	-0.09	0.44	0.08
20170403	0.09	-0.09	0.60	0.09
20170503	0.10	-0.03	0.56	0.08
20170622	0.09	-0.10	0.69	0.10
20170702	0.09	-0.12	0.70	0.11
20170813	0.08	-0.10	0.64	0.10
20170907	0.07	-0.27	0.67	0.11
20171017	0.08	-0.17	0.67	0.11
20171116	0.05	-0.13	0.51	0.09
20171216	0.06	-0.17	0.63	0.12
20180115	0.08	-0.21	0.67	0.12

In the analysis we conducted, the NDVI values of the industrial zones varied between 0.06 and 0.10 and the standard deviation was determined to be approximately 0.10, as it shown in Table 5.2.

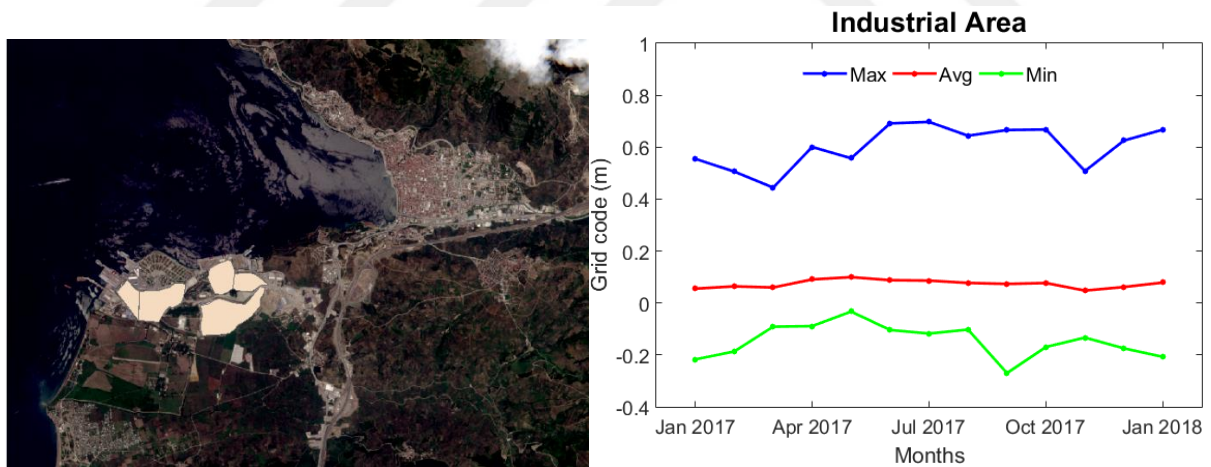


Figure 5.3 Time series analysis of NDVI for the Industrial Area type land cover class.

In the one year period, four new industrial plants were built in the selected region. The minimum and maximum NDVI values vary between -0.22 and 0.70, respectively, as it shown in Figure 5.3.

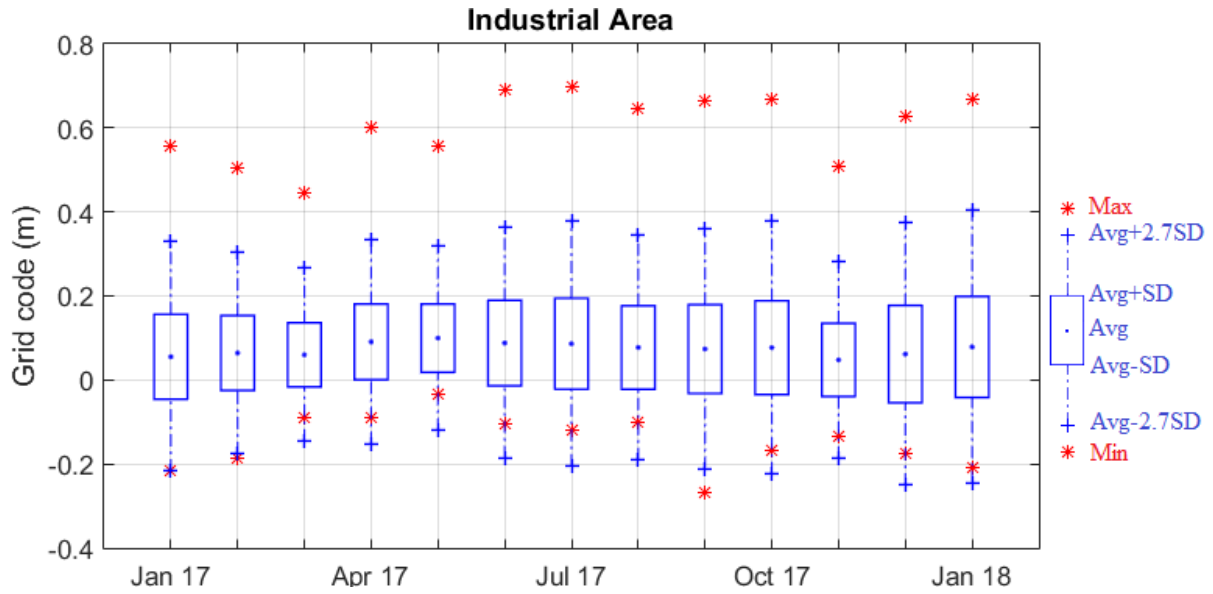


Figure 5.4 SD time series analysis of NDVI for the Industrial Area type class.

Various factories such as Sümerbank Artificial Silk Factory, Tügsaş (production of fertilizers and chemical products), Borusan (pipe production), Çimtaş (steel and iron production), Borçelik (steel production), MKS (chemical industry) are the basis of the industry in Gemlik. Gemport, which has been serving in the region since 1992, has been one of the building blocks of the region with its import and export activities. Industrial areas also have a dynamic structure that shows continuous development. That wide range in NDVI can be caused by the changes in the dynamic structure of some containers within the industrial zone and industrial products such as steel pipes. The time series of the NDVI is shown in Figure 5.4.

5.1.3 NDVI Results of the Forest Type Land Cover Class

In this study, one of the most widely used vegetation indices, NDVI, was used. If the calculated NDVI values are bright; the amount of healthy vegetation is much more. By using NDVI images obtained at different dates, seasonal changes of vegetation can be revealed and the relationship between vegetation change and climate can be established. NDVI information can be derived from each satellite system that makes detection in the near infrared and red regions. In this context, the temporal variation of average NDVI values within the selected forest area in Gemlik region is as in Table 5.3.

Table 5.3 Attribute table of Forest type land cover class.

Date	Avg.	Min	Max	SD
20170113	0.37	-0.15	0.71	0.18
20170202	0.45	-0.11	0.69	0.15
20170301	0.42	0.01	0.61	0.10
20170403	0.49	0.00	0.67	0.08
20170503	0.53	-0.01	0.69	0.06
20170622	0.60	-0.03	0.78	0.07
20170702	0.65	-0.04	0.81	0.08
20170813	0.58	0.00	0.75	0.09
20170907	0.58	-0.03	0.74	0.09
20171017	0.57	-0.09	0.75	0.10
20171116	0.43	0.01	0.67	0.13
20171216	0.46	-0.12	0.74	0.18
20180115	0.45	-0.08	0.74	0.18

As shown in Table 5.3, mean NDVI values ranged between 0.37 and 0.45. While NDVI values are increasing in April, they reach the highest values in July and then decrease in time towards autumn (Figure 5.5).

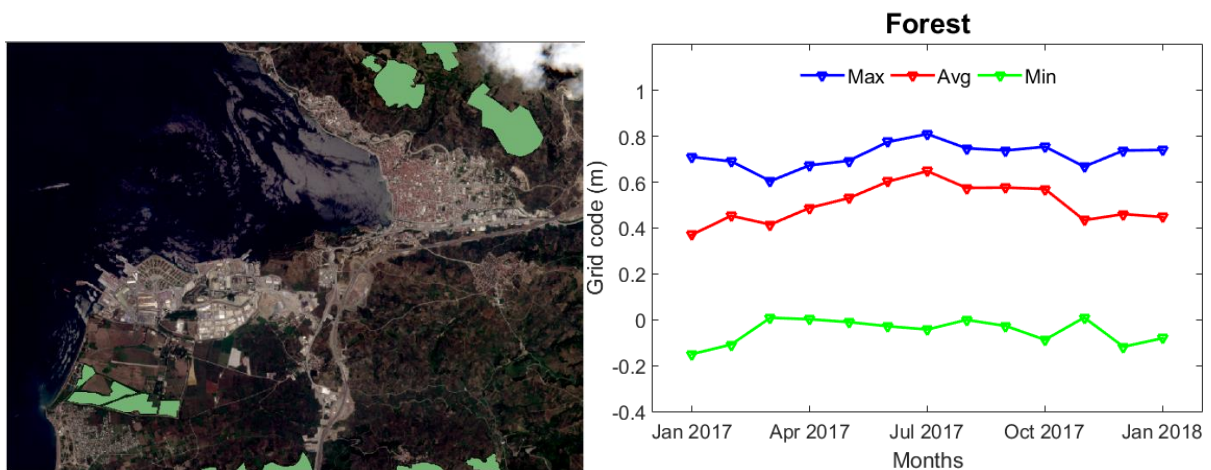


Figure 5.5 Time series analysis of NDVI for the Forest type land cover class.

The standard deviation of NDVI values for the forest area varies between 0.18 and 0.06. While the standard deviation values increase due to the decrease in the chlorophyll content in autumn and winter months, with the increase of chlorophyll amount in the spring and summer shows a decrease in the standard deviation of NDVI values. As shown in Figure 5.6, all of the max NDVI values are within the range of 2.7 sigma and min values are outliers.

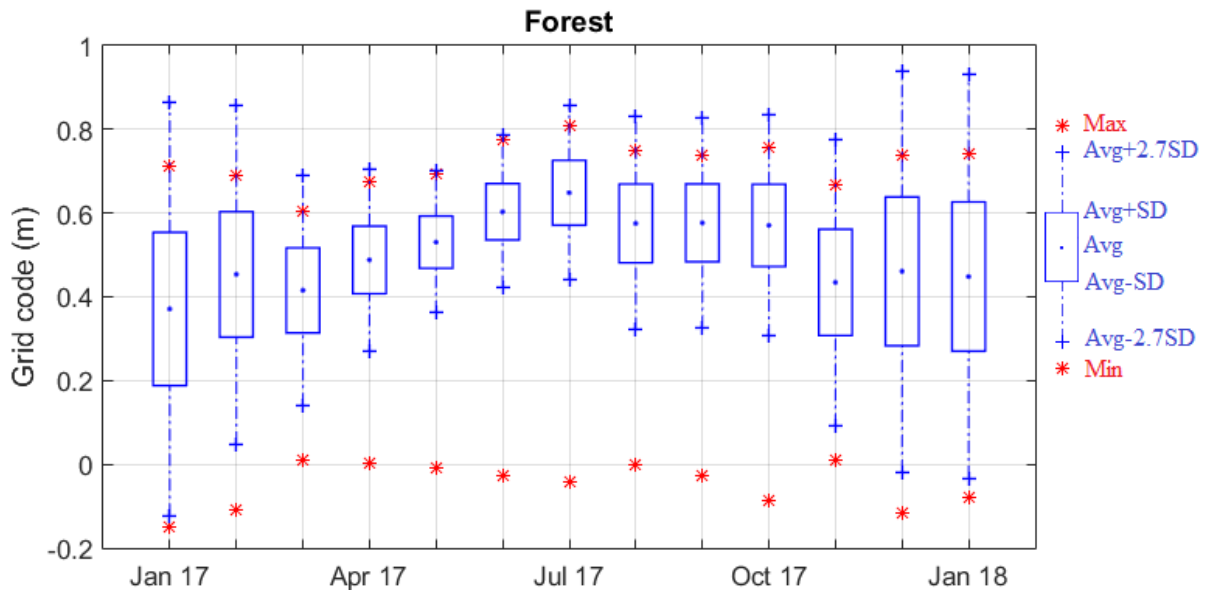


Figure 5.6 SD time series analysis of NDVI for the Forest type class.

5.1.4 NDVI Results of the Buildings Type Land Cover Class

The areas we have selected for the buildings include city center of Gemlik, coastline and villages. The average NDVI values representing this region range from 0.13 to 0.26, in Table 5.4.

Table 5.4 Attribute table of Buildings type land cover class.

Date	Avg.	Min	Max	SD
20170113	0.13	-0.84	1.00	0.12
20170202	0.14	-0.73	0.71	0.11
20170301	0.14	-0.09	0.61	0.10
20170403	0.18	-0.08	0.69	0.11
20170503	0.22	-0.05	0.65	0.13
20170622	0.23	-0.14	0.74	0.16
20170702	0.23	-0.14	0.76	0.16
20170813	0.21	-0.20	0.73	0.14
20170907	0.21	-0.09	0.79	0.15
20171017	0.20	-0.17	0.73	0.14
20171116	0.14	-0.45	0.73	0.11
20171216	0.15	-0.63	1.00	0.13
20180115	0.16	-1.00	1.00	0.14

While the mean NDVI values in the autumn and winter months are between 0.13 and 0.16, they are increasing and varying between 0.18 and 0.26 in spring and summer. The main reason for this situation is that the houses on the coastline and villages are covered with trees and greenery. The increase in the amount of chlorophyll in plants due to the increase of temperatures in the region in spring leads to an increase in NDVI values. The increase in the standard deviation of NDVI values during the summer can also be due to the same reason.

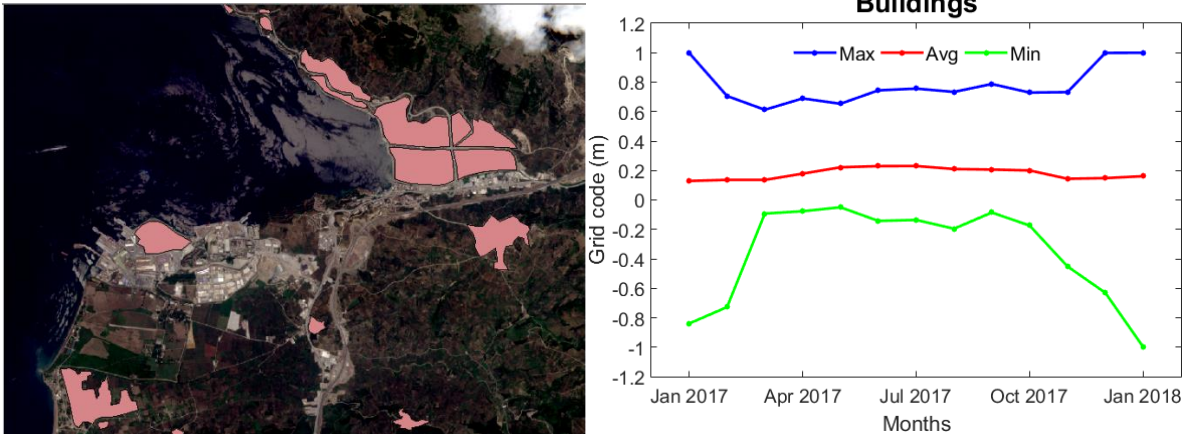


Figure 5.7 Time series analysis of NDVI for the Buildings type land cover class.

Average NDVI results time series illustration of buildings as shown in Figure 5.7. As it seen in figure, the differences between min and max NDVI values vary between -1 and +1. Figure 5.8 shows that these min and max values are mostly not in the 2.7 sigma confidence interval and are outlier.

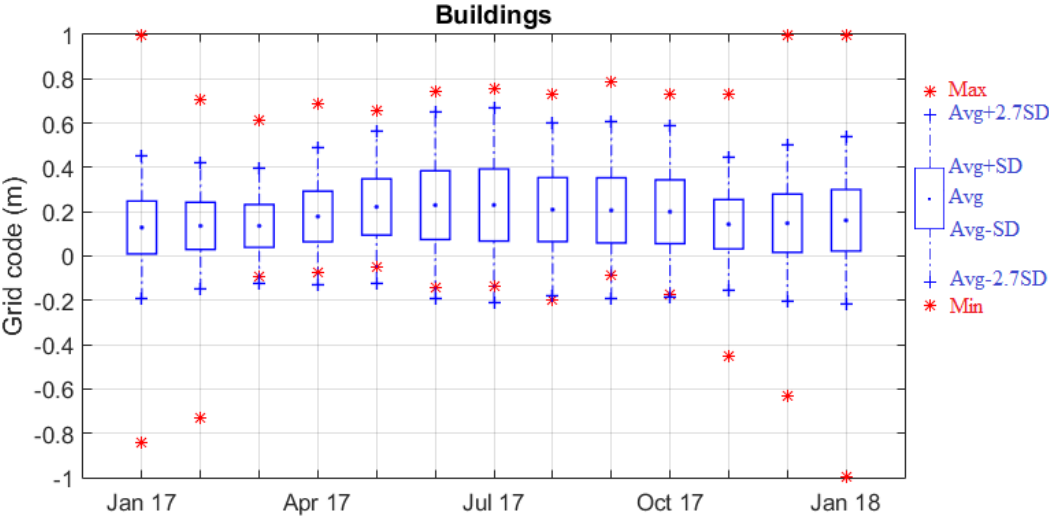


Figure 5.8 SD time series analysis of NDVI for the Buildings type class

5.1.5 NDVI Results of the Agricultural Area Type Land Cover Class

Gemlik region has a total agricultural area of 104353 decares. Considering that the products grown are more than 1 percent of the total agricultural area, 1.77 percent barley, 9.91 percent wheat berry, 1.26 percent peach and 78.35 percent olive production is realized (Table 5.5).

Table 5.5 Most common products of Agricultural Area in Gemlik.

Products	Year	Decare	Percentage
Barley	2017	1848	1.77
Wheat berry	2017	10339	9.91
Peach	2017	1316	1.26
Olive	2017	81761	78.35
Total	2017	104353	100.00

As shown in Figure 5.9, average NDVI values start to increase in April. And, there is a sharp decline in June. This may be due to the fact that agricultural harvests such as barley, wheat and peach are grown in the middle of June. The average NDVI values, which increased again after June, fallen sharply again in November. The main reason for this is that olive trees, which cover about 78 percent of the total agricultural area, harvested in November.

Table 5.6 Attribute table of Agricultural Area type land cover class

Date	Avg.	Min	Max	SD
20170113	0.42	-0.06	0.68	0.15
20170202	0.41	-0.05	0.67	0.14
20170301	0.38	0.00	0.62	0.11
20170403	0.50	0.02	0.77	0.11
20170503	0.49	0.06	0.72	0.10
20170622	0.41	0.00	0.71	0.11
20170702	0.47	-0.01	0.78	0.12
20170813	0.42	-0.02	0.80	0.11
20170907	0.43	-0.02	0.75	0.12
20171017	0.47	-0.04	0.80	0.14
20171116	0.39	0.00	0.71	0.11
20171216	0.49	-0.09	0.78	0.13
20180115	0.53	-0.05	0.78	0.12

The average NDVI values in the selected areas for agricultural products ranged from 0.38 to 0.53 (Table 5.6). The diversity of cultivated agricultural products, the difference in the planting, fertilizing and harvesting dates affect the results of these agricultural products obtained using from satellite images.

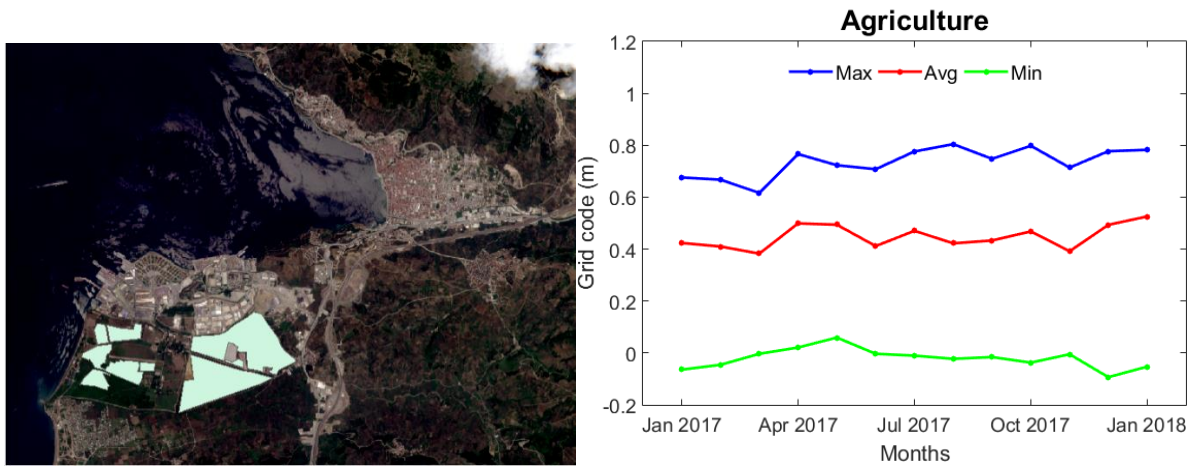


Figure 5.9 Time series analysis of NDVI for the Agricultural Area type land cover class.

Standard deviation values, as in the forest areas, decreases towards the summer season, but increase towards the winter season. Max values obtained for agricultural areas were generally in the range of 2.7 sigma confidence, while min values were found to be outliers (Figure 5.10).

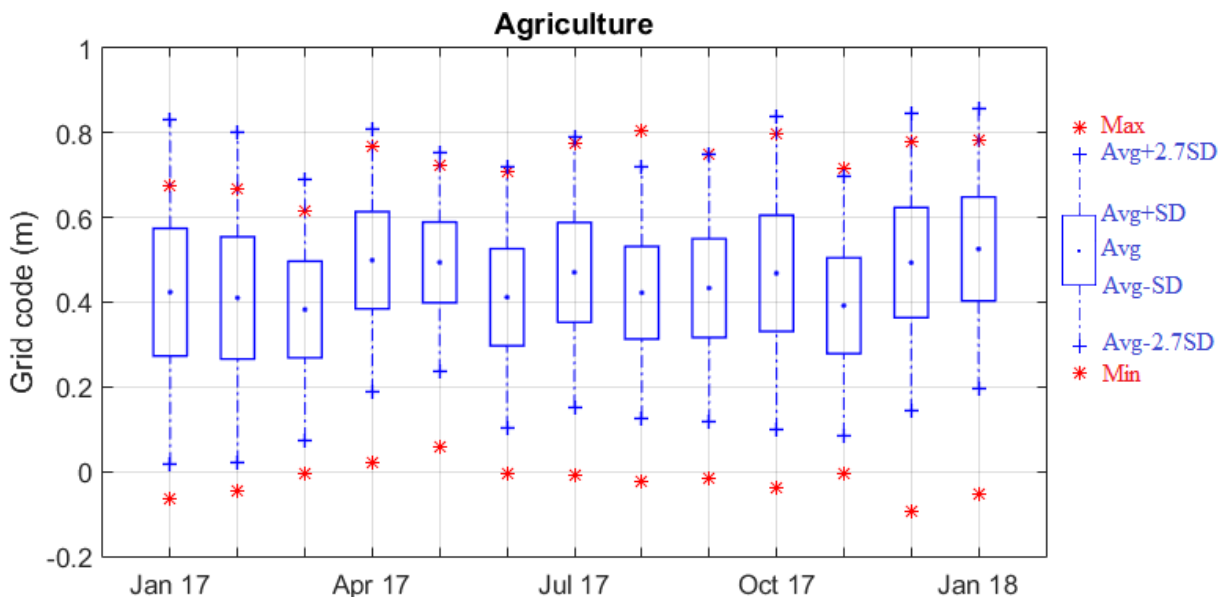


Figure 5.10 SD time series analysis of NDVI for the Agricultural Area type class.

5.1.6 NDVI Results of the Sea Type Land Cover Class

The large number of cloudy days in Gemlik region in January 2018 caused difficulties in the selection of satellite images. The area chosen for the sea class was first selected to cover all borders on the image. In the satellite image of January 2018, the clouds covering a part of the sea caused excessive deviation in the values we obtained for the sea class. This error source, which removes the process from the realism, has been fixed by keeping it outside the selection area of the cloudy zone. The average NDVI values for the sea are in the range of -0.32 to -0.07 as shown in Table 5.7.

While the average NDVI values decreasing to -0.32 in winter, they are increasing up to -0.07 during summer. The snow and rain water fallen during the winter, reach the streams and then they fall into the sea. Before these snow and rain water reach the seas, they also contact with the soil (such as fertilizer used in agriculture) and carry some nutrients included in soil. In 2017, approximately 2780 tons of fertilizer was used in Gemlik. This means, snow and rain water falling into the sea with these nutrients causes an increase in plant products grown in the seas.

Table 5.7 Attribute table of Sea type land cover class.

Date	Avg.	Min	Max	SD	Avg-1SD	Avg+1SD	Avg-2.7SD	Avg+2.7SD
20170113	-0.32	-0.49	0.31	0.02	-0.34	-0.29	-0.38	-0.25
20170202	-0.27	-0.36	0.29	0.02	-0.29	-0.26	-0.32	-0.22
20170301	-0.22	-0.28	0.38	0.01	-0.23	-0.20	-0.25	-0.18
20170403	-0.20	-0.27	0.22	0.02	-0.22	-0.19	-0.24	-0.16
20170503	-0.12	-0.19	0.18	0.01	-0.13	-0.11	-0.16	-0.08
20170622	-0.20	-0.47	0.24	0.04	-0.24	-0.17	-0.30	-0.11
20170702	-0.07	-0.27	0.28	0.02	-0.09	-0.06	-0.13	-0.02
20170813	-0.26	-0.34	0.24	0.02	-0.28	-0.24	-0.32	-0.21
20170907	-0.26	-0.43	0.35	0.02	-0.28	-0.23	-0.32	-0.19
20171017	-0.29	-0.51	0.50	0.03	-0.32	-0.26	-0.36	-0.22
20171116	-0.23	-0.29	0.20	0.02	-0.24	-0.21	-0.27	-0.18
20171216	-0.28	-0.41	0.24	0.02	-0.30	-0.25	-0.34	-0.22
20180115	-0.30	-0.40	0.31	0.02	-0.32	-0.27	-0.36	-0.23

The increase in the amount of algae in the seas brings about an increase in NDVI values. The min, max and average NDVI values of the selected area for the sea are as shown in Figure 5.11.

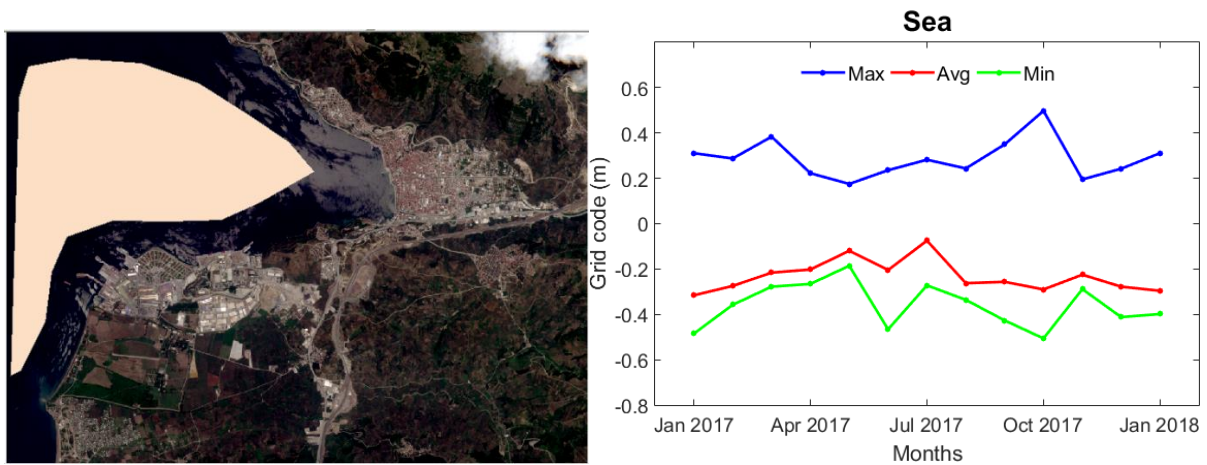


Figure 5.11 Time series analysis of NDVI for the Sea type land cover class.

As shown in Figure 5.11, the average NDVI values for the selected sea region increased towards the summer. A sharp decrease was observed in average NDVI on the image of 22nd of June 2017. When the rainfall data of the region were examined, it was observed that the Gemlik region received extreme rainfall for 3 days on June 19-21, 2017. The changes created by the weather conditions were at a level that can be distinguished on the natural images.

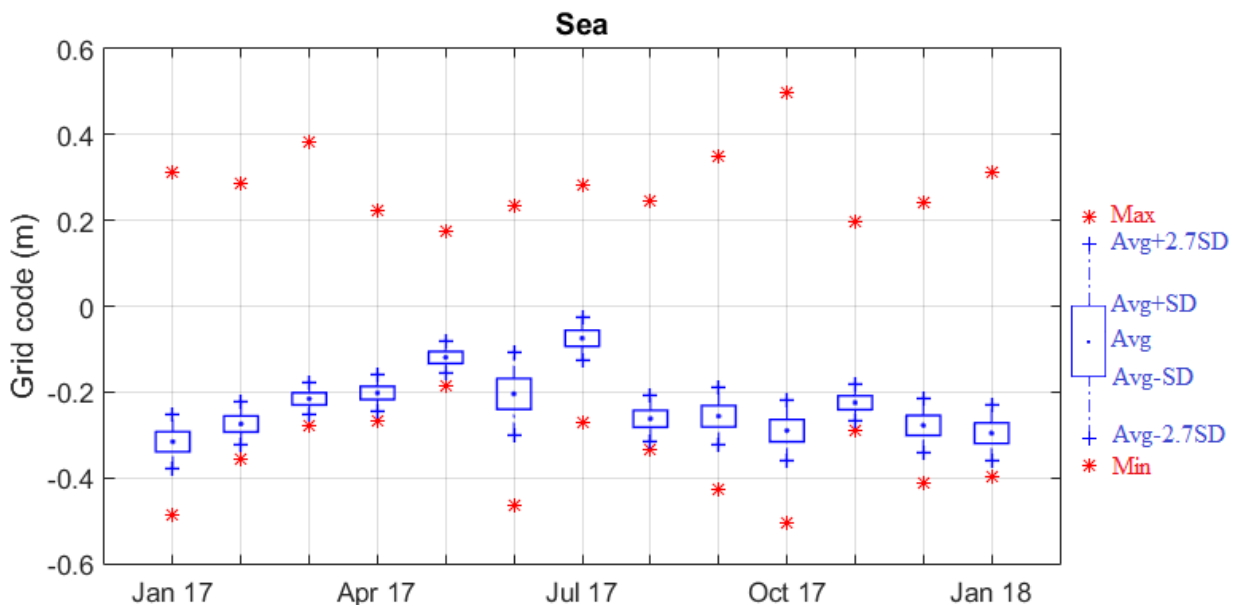


Figure 5.12 SD time series analysis of NDVI for the Sea type class.

None of the minimum and maximum NDVI values for the sea are in the range of 2.7 sigma confidence as seen in Figure 5.12. The main reason is that the selected area for the sea surrounds a port with active and high utilization capacity. Freight ships and the containers they carry to the port can be caused different NDVI values. When the standard deviation values are taken into consideration, there is no significant change, but the increase in the standard deviation in June was observed. However, considering the other classes, sea class NDVI values are the lowest with about 0.02 standard deviations.

5.2 DISCUSSION

Classification is a decision making process, that issued in many disciplines of sciences and technology. In case of multispectral image classification, the aim is to assign pixels to the pre-defined type of land cover. However; object's reflectance for each pre-defined land cover type could be quite similar. This fact limits the accuracy of the image classification.

In this study, a set of pre-defined types of land cover were manually selected. The time dependent variations of the NDVI for selected types of land cover were investigated.

Figure 5.13 shows time series of the average NDVI for investigated land cover types. For the sea class the NDVI varies between -0.32 and -0.07; For the industrial areas the range of variations is much smaller, i.e., between 0.05 and 0.10. For the Buildings type the index varies between 0.13 and 0.23; For the Roads type between 0.11 and 0.26. And finally, for the agricultural areas the NDVI varies between 0.38 and 0.53, and for the forested areas between 0.37 and 0.65. The graphs in Figure 5.13 reveals a few important facts:

1. The land cover agriculture and forests are basically the same in terms of the NDVI values during a year, except for the summer months, when the NDVI for forest class is significantly higher than that of the agriculture. The increase in the number of sunny days and the increase in the amount of chlorophyll cause an increase in NDVI values. The increase in the amount of chlorophyll in the forest areas is more intense than the agricultural products, and some agricultural products are harvested in the summer months. Therefore, in the summer months, the difference between the NDVI values of agricultural products and forest areas is opened.

2. The land cover class Road and Buildings follows almost identical pattern during the investigated period. A noticeable culmination of the NDVI during summer months can be explained by the fact that both classes include a certain percentage pixels representing vegetation. In turns, this translates into an elevated level of NDVI for both classes.

3. The Industrial class appears to be the most stable during the investigated period. This was quite anticipated, because Industrial class is almost totally antropogenic by definition and its spectral signature does not change over time. The standard deviation of the NDVI for the class can be considered as a measure of errors in the remote sensing data from this particular satellite program. The standard deviation for this class equals to 0.10. This means that the threshold of the sensitivity or ability to detect changes in land cover is of this level. In other words, if the magnitude of change for a certain class is one sigma or less, one cannot say if the change is genuine or it is just an error.

4. The analysis results show that the standard deviation for the sea is very small. Rain and snow waters reach the rivers and then pour into the sea. The nutrients it carries during this trip increase the amount of algae in the seas. This algae, which is an important source of food for living creatures, can be distinguished by NDVI values that increase in spring and summer. There was a sudden decline in NDVI values of the image dated 22 June. When the meteorological data were analysed, it was found that the region received excessive rainfall during 19th to 21st of June. Some chemical wastes in industrial facilities may be mixed into the sea with these rains.

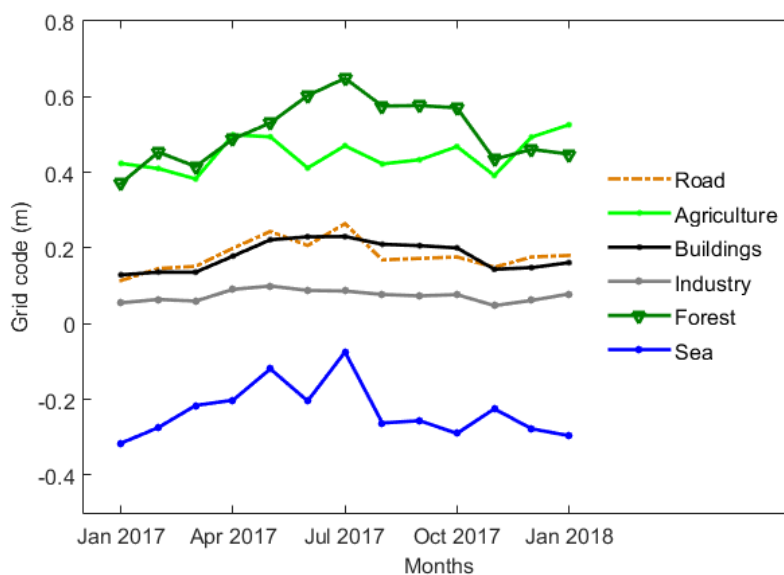


Figure 5.13 Time series of average NVDI of classes.

When the industrial areas were examined, it was determined that there was no significant change. The jumps in the maximum and minimum values are due to the dynamic structure of the region. The situation for buildings varies slightly. Because the area of choice was made from the city center, coastline and villages. The green and wooded surroundings of the garden houses bring about an increase in NDVI values in the spring. For a more detailed analysis, more detailed results could be obtained if individual vector layers were formed instead of joining the selection regions under a single vector layer. It is also same for the road class. Asphalt, surface treatment and unpaved roads were also combined in a single vector layer. Due to the construction materials, these objects with different reflection values can be considered as different vector layers for better analysis.

The reflection values of agricultural lands and forest areas are close to each other and possible to interfere. Similar characteristics, increased chlorophyll amounts due to the improvement of weather conditions cause an increase in NDVI values. The diversity of agricultural products, deciduous and evergreen trees affect the reflection values. In general, agricultural products drop leaves but, olive trees which have 78 percent of usage in total agricultural area in Gemlik, are evergreen. Therefore, for a more detailed analysis of agricultural products, it is necessary to evaluate the product in specific vector layers. If such studies are supported by on-site observations, the standard deviation of the data on the products will be considerably reduced.



CHAPTER 6

CONCLUSION

In this study, the temporal variations of the spectral characteristics of LULC over a period of approximately one year (2017) have been studied. The Bursa Gemlik, Turkey region was the selected as AOI. The region includes different LCLU types, including industrial, agricultural, forest, building, road and water body. These different types of objects represented by the NDVI values were examined as time series.

The analysis of the time series allows to formulate the following conclusions:

1. Considering standard deviation (SD) of the average value of NDVI as an indicator of the “stability” over time of the spectral characteristics of investigated class, the smallest the most stable appears to be water body (sea water in this case) with the average $SD = 0.02$. The largest $SD = 0.31$ was recorded for the Roads class. As anticipated, SD for the Industrial area class was 0.1. Since this class was selected as the most stable class the $SD = 0.1$ can be accepted as a level of the uncertainty determined by the unperfect calibration of the satellite data and errors caused by the atmosphere.
2. It is possible to use the conclusion No 1 as a guide to develop an accuracy measure of the remote sensing image classification, and even build a correction algorithm for compensating the residual errors of calibration and atmosphere influences.
3. Natural LULC classes, including Agriculture and Forest follow a seasonal pattern: The highest NDVI readings were recorded for the summer months (May, Jun and July), and the lowest during the autumn, winter and early spring. However the variations for Agriculture class were less pronounced, than for the Forest class. This would suggest that the test samples selected in this study for the Forest class included deciduous forest.
4. The Building class exhibits an elevated level of $SD = 0.13$, which one would not expect. However, closer look at the selected test samples for the class revealed that the samples contain

some mixed pixels. These mixed pixels include various fraction of vegetation which tends to follow a seasonal pattern

5. The Sea or water body class exhibits a relatively large range of values of NDVI (-0.32 to -0.07). After close inspection of the images it was found that water in the Marmara Sea is mixed with water discharged by rivers and streams found in the AOI. The discharging water, after heavy precipitation, contains many both organic and mineral contaminants. This include some residual of fertilizer used by farmer. In turn, fertilizer reach coastal waters in are good environment for development of algae species which contain chlorophyll. This would explain that the rising level of NDVI, and in general seasonal pattern of the NDVI of this Sea class.

6. Sentinel 2 data can be used to monitor LULC changes, which is important to monitor human impact on the environment. This kind of activities can be conducted for regional scale at a very low costs and to the large extend in a semi- or even an automatic fashion.

7. Overall, this exploratory study produced some interesting results warranting another more comprehensive and focused study of the variability of spectral characteristics of LULC over time and their correlation with some meteorological and economic factors.

Agriculture has great importance not only in local or country but also globally. Countries have to make the planning and management of agricultural resources prospectively as their population increases. Turkey, a country that was known as more agricultural potential than the industry until the last decade, but today shows a tendency to reverse this situation. Therefore, it is necessary to know the existing agricultural product potentials and to use them in the most effective way in determining economic needs and decisions depending on the increase of urban and rural settlements. Thanks to the developing space and computer technology, human beings are able to make important agricultural projects with easier and high accuracy. In addition to this, with the help of Geographic Information Systems, complex analyzes are performed and the quality and quantity of agricultural products are important. In this study, the agricultural potential in Gemlik which is a district above the national average in agriculture and industry is examined with 1 year remote sensing data. The changes in 2017 were examined by applying the NDVI index.

REFERENCES

- Acker J G, McMahon E, Shen S, Hearty T and Casey N** (2009) Time Series Analysis of Remotely Sensed Seawifs Chlorophly In River Influenced Coastal Regions. *EARSeI eProceedings*, 8: 114-139.
- Altunkaya Z ve Yastikli N** (2011) Ortogörüntüler Yardımıyla Nesne Tabanlı Sınıflandırma Yöntemi Kullanılarak Öznitelik Çıkarımı, *TMMOB Coğrafi Bilgi Sistemleri Kongresi*, 31 Ekim - 4 Kasım 2011, Antalya, 1-7.
- Aplin P and Smith G M** (2008) Advances in object-based image classification. *ISPRS Conference*, 2008, Beijing, The International Archives of the Photogrammetry, Remote Sensing and Spatial Information Sciences, 37: 725–728.
- Belgiu M and Csillik O** (2018) Sentinel-2 Cropland Mapping Using Pixel-Based and Object-Based Time-Weighted Dynamic Time Warping Analysis. *Remote Sens. Environ.*, 204: 509–523.
- Blaschke T** (2010) Object based image analysis for remote sensing. *ISPRS Journal of Photogrammetry and Remote Sensing*, 65 (1): 2-16.
- Çelik H** (2006) İstanbul Sarıyer İlçesine Ait Uzaktan Algılama Uydu Verileri ile Mekansal Veri Analizleri. *Yüksek Lisans Tezi*, Çanakkale Onsekiz Mart Üniversitesi, Fen Bilimleri Enstitüsü, Çanakkale, 170 s.
- Çölkesen İ** (2009) Uzaktan Algılamada İleri Sınıflandırma Tekniklerinin Karşılaştırılması ve Analizi. *Yüksek Lisans Tezi*, Gebze Yüksek Teknoloji Enstitüsü, Mühendislik ve Fen Bilimleri Enstitüsü, Jeodezi ve Fotogrametri Mühendisliği Anabilim Dalı, 153 s.
- Drusch M, Del Bello U, Carlier S, Colin O, Fernandez V, Gascon F, Hoersch B, Isola C, Laberinti P and Martimort P** (2012) Sentinel-2: ESA's Optical High-Resolution Mission for GMES Operational Services. *Remote Sens. Environ.*, 120: 25–36.
- Duran C** (2007) Uzaktan algılama teknikleri ile bitki örtüsü analizi. *Doğu Akdeniz Ormanlık Araştırma Müdürlüğü DOA Dergisi*, 13: 45–46.
- Ekercin S** (2007) Uzaktan algılama ve coğrafi bilgi sistemleri entegrasyonu ile Tuz Gölü ve yakın çevresinin zamana bağlı değişim analizi. *Doktora Tezi*, İstanbul Teknik Üniversitesi, Fen Bilimleri Enstitüsü, İstanbul, 182 s.
- Harrison B A and Jupp D L B** (1989) *Introduction to remotely sensed data*. ISBN: 0-643-04991-6, CSIRO Publications, Canberra, Australia, 141 pp.

REFERENCES (continued)

- Immitzer M, Vuolo F and Atzberger C** (2016) First Experience with Sentinel-2 Data for Crop and Tree Species Classifications in Central Europe. *Remote Sensing*, 8: 1-27.
- Inglada J, Arias M, Tardy B, Hagolle O, Valero S, Morin D, Dedieu G, Sepulcre G, Bontemps S, Defourny P and Koetz B** (2015) Assessment of an Operational System for Crop Type Map Production Using High Temporal and Spatial Resolution Satellite Optical Imagery. *Remote Sens.*, 7: 12356-12379.
- Jehnsen J R** (1996) *Introductory digital image processing: A remote sensing perspective*. 2nd Edition, ISBN-10: 0131453610, Prentice Hall, New Jersey, 526 pp.
- Karakış S** (2005) Quickbird Örneğinde Yüksek Çözünürlüklü Uydu Görüntüsü Üzerinden Kentsel Ayrıntıların Otomatik ve Manuel Çıkarımı Üzerine Bir Uygulama. *Yüksek Lisans Tezi*, Zonguldak Karaelmas Üniversitesi, Fen Bilimleri Enstitüsü, Jeodezi ve Fotogrametri Mühendisliği Anabilim Dalı, Zonguldak, 99 s.
- Lillesand T M, Kiefer R W and Chipman J W** (2007) *Remote sensing and image interpretation*. 6th Edition, ISBN-10: 9780470052457, John Wiley & Sons: New York, 804 pp.
- Marangoz A M, Karakış S, Oruç M ve Büyüksalih G** (2005). Nesne-tabanlı görüntü analizi ve IKONOS pan-sharpened görüntüsünü kullanarak yol ve binaların çıkarımı, *10. Türkiye Harita Bilimsel ve Teknik Kurultayı*, 28 Mart-01 Nisan 2005, Ankara, 1-6.
- Mather P M and Koch M** (2011) *Computer Processing of Remotely – Sensed Images: An Introduction*. 4th Edition, ISBN: 978-0-470-74239-6, John Wiley & Sons, USA, 460 pp.
- Musaoğlu N** (1999) Elektro-Optik ve Mikrodalga Algılayıcılardan Elde Edilen Uydu Verilerinden Orman Alanlarında Meşcere Tiplerinin ve Yetiştirme Ortamı Birimlerinin Belirlenme Olanakları. *Doktora Tezi*, İstanbul Teknik Üniversitesi, İstanbul, 112 s.
- Myint S W, Gober P, Brazel A, Grossman-Clarke S and Weng Q H** (2011) Per-pixel vs. object-based classification of urban land cover extraction using high spatial resolution imagery. *Remote Sensing of Environment*, 115 (5): 1145-1161.
- Paine D P and Kiser J D** (2012) *Aerial Photography and Image Interpretation*. 3rd Edition, ISBN: 978-0-470-87938-2, John Wiley & Sons Pres., New Jersey, 648 pp.
- Ramachandra T V and Kumar U** (2004) Geographic resources decision support system for land use, land cover dynamics analysis. *Proceedings of the FOSS/GRASS Users Conference*, 12-14 September 2004 Bangkok, Thailand, 1-15.
- Rapinel S, Mony C, Lecoq L, Clément B, Thomas A and Hubert-Moya L** (2019) Evaluation of Sentinel-2 Time-Series for Mapping Floodplain Grassland Plant Communities. *Remote Sensing of Environment*, 223: 115–129.

REFERENCES (continued)

- Schiewe J, Tufte L and Ehlers M** (2001) Potential and problems of multi-scale segmentation methods in remote sensing. *GIS-Zeitschrift für Geoinformations systeme*, 6: 34-39.
- Schowengerdt R** (1997) *Remote Sensing: Models and Methods for Image Processing*. Second Edition, ISBN: 9780080516103, Academic Press, Arizona, 522 pp.
- Song X, Yang C, Wu M, Zhao C, Yang G, Hoffmann W C and Huang W** (2017) Evaluation of Sentinel-2A Satellite Imagery for Mapping Cotton Root Rot. *Remote Sensing*, 9: 1-17.
- Uça Avcı Z D ve Sunar F** (2010) Çok-Zamanlı Optik Veri Setinin Tarımsal Haritalama Amaçlı Nesne-Tabanlı Sınıflandırılması: Türkgeldi Örneği. *III. Uzaktan Algılama ve Coğrafi Bilgi Sistemleri Sempozyumu*, 12-15 Ekim 2010, Gebze, 268-272.
- [URL-1] <<https://sentinel.esa.int/web/sentinel/missions/sentinel-2>>, Last Visit: 07.02.2019.
- [URL-2] <http://www.esa.int/Our_Activities/Observing_the_Earth/Copernicus/Sentinel-2/Sentinel-2_delivers_first_images>, Last Visit: 07.01.2019.
- [URL-3] <http://www.esa.int/Our_Activities/Observing_the_Earth/Copernicus/Sentinel-2/Introducing_Sentinel-2>, Last Visit: 17.12.2018.
- [URL-4] <<https://sentinels.copernicus.eu/web/sentinel/missions/sentinel-3/ground-segment>>, Last Visit: 07.02.2019.



CURRICULUM VITAE

She was born in Bolu, Turkey, in April 1992. In 2015, she has received her bachelor's degree from Yildiz Technical University. After than working in private companies for a while, she has started to study her master education at Zonguldak Bulent Ecevit University and continues to postgraduate education.

ADDRESS: Incivez Mahallesi, Üniversite Caddesi,
No:71 Kaya Apartmanı, Kat: 5, Daire 13
Zonguldak / Türkiye

Phone: (+90) 531 672 07 92

E-mail: bakiogluoyaburcu@gmail.com